This is to certify that the
thesis entitled

EXPERIMENTAL AND NUMERICAL INVESTIGATIONS OF THE SHEET HYDRAULIC BULGE TEST FOR ALUMINUM ALLOYS

presented by

SHREYAS CHITTA NAGARAJ

has been accepted towards fulfillment
of the requirements for the

M.S. degree in MECHANICAL ENGINEERING

F. Barlat

Major Professor's Signature

12/16/2005

Date

EXPERIMENTAL AND NUMERICAL INVESTIGATIONS OF THE SHEET HYDRAULIC BULGE TEST FOR ALUMINUM ALLOYS

By

Shreyas Chitta Nagaraj

A THESIS

Submitted to
Michigan State University
in partial fulfillment of the requirements
for the degree of

MASTER OF SCIENCE

Department of Mechanical Engineering

2005

ABSTRACT

EXPERIMENTAL AND NUMERICAL INVESTIGATION OF THE SHEET HYDRAULIC BULGE TEST FOR ALUMINUM ALLOYS

By

Shreyas Chitta Nagaraj

The bulge test has been identified as a standard method for obtaining stress-strain relationships through large plastic strain in biaxial tension and the utilization of this information in formability assessment. A major advantage of the hydraulic bulge test over the more conventional uniaxial tensile test is that the stress-strain curve extends to the range of effective strain found in many forming applications. However dynamic measurement of various parameters during the sheet metal bulge test poses a challenge and requires specially designed and customized equipment and not to mention careful attention to detail in order to get accurate results. Typical bulge test stress-strain curves are presented for a variety of aluminum sheet alloys and compared with tensile curves obtained from similar tests conducted by 'Aluminum Company of America' (ALCOA). This study describes the theoretical basis for the test, the test equipment, the measurement system, the data processing system and the various challenges faced during the testing process and how it was overcome. The study also describes a numerical simulation for the sheet metal hydroforming using the explicit finite element code LS-Dyna 3D and the results compared to the experimental results. It is anticipated that a facility of this kind will have wide application in studying the basic behavior of sheet alloys, particularly those which must be formed at high levels of strain such as alloys used in manufacturing and automotive applications of aluminum sheet.

Dedicated

To my parents

ACKNOWLEDGEMENTS

First and foremost I would like to thank my adviser Dr. Farhang Pourboghrat for his support and encouragement throughout the course of my study at MSU, without his support it would have been impossible to reach this stage of my career. Special thanks to my colleague Nader Abedrabbo whose support played a vital role in the successful completion of my MS thesis. I would also like to thank Dr. Gary Cloud for sharing his valuable experience and practical knowledge of experimental work with me. Special thanks to machine shop supervisors Roy Bailiff, Michael Mclean and Gerard Westover who helped me immensely for all the fabrication work involved in this study. Special thanks to the National Instruments Technical Support team.

Last but not the least I would like to thank my Parents, my sister and brother in India, Uncles Paramesh Nalval, Sriram Sringari, Aunts Bharathi Nalval, Nirmala Sringari, my cousins, and my grandmother for their constant support and encouragement.

TABLE OF CONTENTS

LIST OF TABLES

LIST OF FIGURES

NOTE: Images in this thesis are presented in color

LIST OF ABREVIATIONS

$\varepsilon_{1,2,3}$ - True Strain along the x, y, z directions

ε_t - Thickness strain

$\sigma_{1,2,3}$ - True Stress along the x, y, z directions

P – Pressure on the sheet

R – Radius of curvature of the sheet

t - Thickness of the sheet

a – distance from the spherometer probe to each spherometer leg

h – Difference in height between the center of the sheet and the spherometer leg

D – Instantaneous chord length of sheet at the extensometer tip

D_0 – Initial chord length of sheet

Φ – Yield function

$S_{1,2,3}$ – Principal values of stress deviator

L – Fourth order linear operator

C_1, C_2, C_3, α_x, α_y, α_{z1} – Coefficients that describe the anisotropy of material

σ_b - flow stress

R_θ – Plastic anisotropy parameters where $\theta = 0^0, 45^0, 90^0$

m – Strain rate sensitivity index

n – Strain hardening exponent

K - Strength hardening coefficient

CHAPTER 1

INTRODUCTION

The hydraulic bulge test is used to determine stress-strain properties of sheet metal under Biaxial Tension [1]. The most significant advantage of the hydraulic bulge test over the more conventional uniaxial tensile test is that the stress strain curve extends to the range of effective strain found in many forming applications. Apart from this the Hydraulic Bulge test can be used over the tensile test in the following situations:

1. For determining the plastic properties of materials that exhibit little ductility [2]
2. For investigating plastic properties at low strains in materials that exhibit large Luders Elongation [2]
3. For determining normal anisotropy in materials that do not follow Hill's Theory [2]
4. For determining work hardening characteristics at the high strains at which failure processes develop during press forming [2]

The Bulge test consists of sheet (blank) clamped around the edges and deformed by pressure applied to one side of the sheet, as shown in Figure 1.1. Deformation occurs through the blank with 2D plane strain at the edge to biaxial strain at the pole (center of the specimen).

The hydraulic bulging equipment consists of a blank, blank holder, draw bead and fluid pressure to deform the specimen. The test equipment mainly comprises of an extensometer, a spherometer, a pressure accumulator, a pressure controller with transducer, a control system to dynamically control the pressure and a computer with data acquisition systems.

The blank is held between the draw bead and the blank holder and hydraulic pressure is applied to one side of the blank, the blank continues to deform as the applied pressure increases and finally fails. As the sheet is being deformed the thickness of the sheet reduces with the thinnest section being at the center. The central region continues to deform in an approximately uniform manner until the sheet ruptures. For an isotropic sheet the strains along 2 orthogonal directions in the same plane are equal to each other, whereas for an anisotropic sheet the strains along the orthogonal directions are different and hence measurement along both directions becomes necessary. In this study the sheet is assumed to be isotropic and hence measurement along one direction is performed.

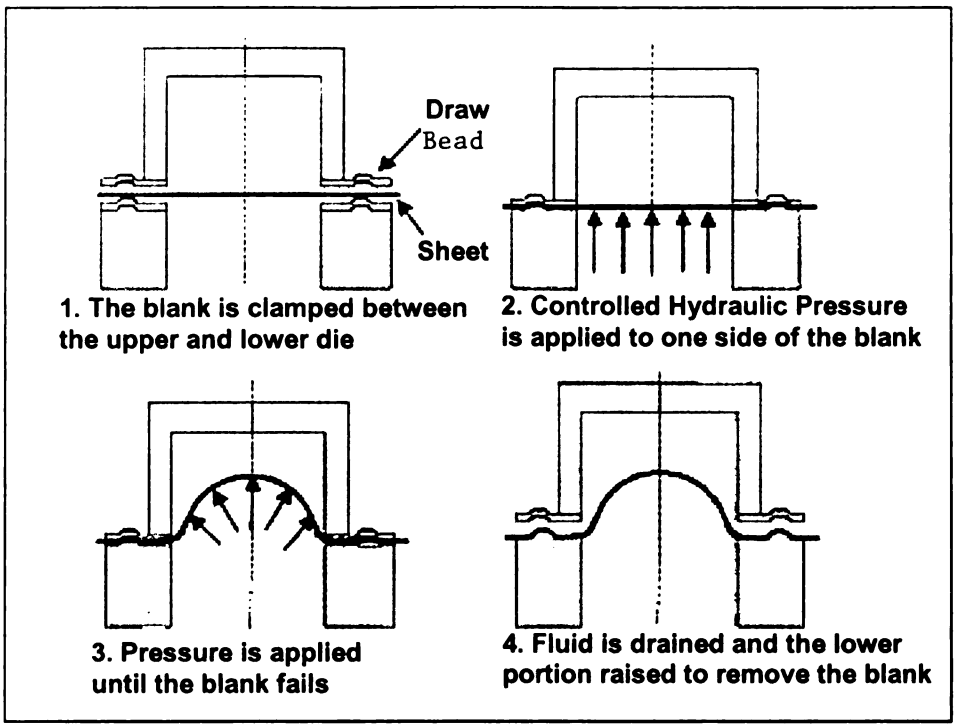

Fig 1.1 shows the schematic of the hydraulic bulge test

1.1 Measurement of True Stress and True Strain

The test is more complicated than the Uniaxial tensile test because the stress and strain can only be determined from the measurement of Pressure, Curvature and the Extension in the center of the disc. The true stress is obtained from the pressure and curvature measurements whereas the true strain is obtained from the measurement of the extension in the center of the bulge.

It was found during experimentation that the actual stress-strain curve obtained from the test is very sensitive to the measurement of the above 3 parameters i.e Pressure, Radius of Curvature and the Extension.

For an Isotropic material the surface strains at the pole by symmetry are equal [1], the principal strains are then in the ratio of:

$$\varepsilon_1 : \varepsilon_2 : \varepsilon_3 = 1:1:-2 \qquad (1.1)$$

Where $\varepsilon_1 = \varepsilon_2 = \varepsilon$, are the membrane strains, and $\varepsilon_3 = \varepsilon_t$ is the thickness strain. Assuming that the volume is constant during plastic deformation we have

$\varepsilon_t = -(\varepsilon_1 + \varepsilon_2)$.

Similarly, the principal stresses are in the ratio of:

$$\sigma_1 : \sigma_2 : \sigma_3 = 1:1:0 \qquad (1.2)$$

Where $\sigma_1 : \sigma_2 = \sigma$ are the membrane stresses, and σ_3 is the through thickness stress. We neglect the effect of hydraulic pressure and assume that σ_3 is zero. The gage area in the test is assumed to be spherical and located at the center of the specimen, as shown in Fig. 1.2. This area is stretched by an approximately uniform biaxial membrane stress. The gage area deforms approximately as a spherical shell of current radius of curvature, R, and current thickness, t, as shown in Fig. 1.3. The membrane stress is a function of R, t and current pressure P.

$$\sigma = \frac{PR}{2t} \qquad (1.3)$$

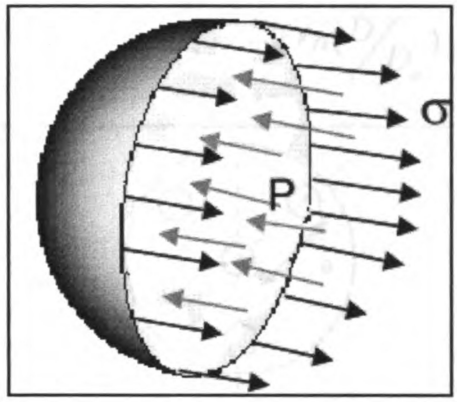

Fig 1.2 shows the spherical system used to measure the Stress

A spherometer is used during the test to measure the radius of curvature, R as shown in figure (1.3)

$$R = \frac{(a^2 + h^2)}{2h} \tag{1.4}$$

The current thickness t is evaluated in terms of the initial thickness t_o and the current thickness strain ε_t

An extensometer is used to measure the strain; it consists of 2 probes which initially rest on the original sheet a distance D_o apart, as shown in Fig. 1.4. As the sheet deforms, the extensometer probes move away from each another and indicate the current length of the gage, D. To calculate strain it is necessary to make the assumption that there is no change in volume and therefore the thickness strain in this area can be given by equation (1.5). The thickness strain obtained from equation 1.5 is a negative quantity and by convention for the bulge test a plot of σ vs $-\varepsilon_t$ is plotted to obtain the true stress strain curve.

$$\varepsilon_t = -2\,\ell n(D/D_o) \qquad (1.5)$$

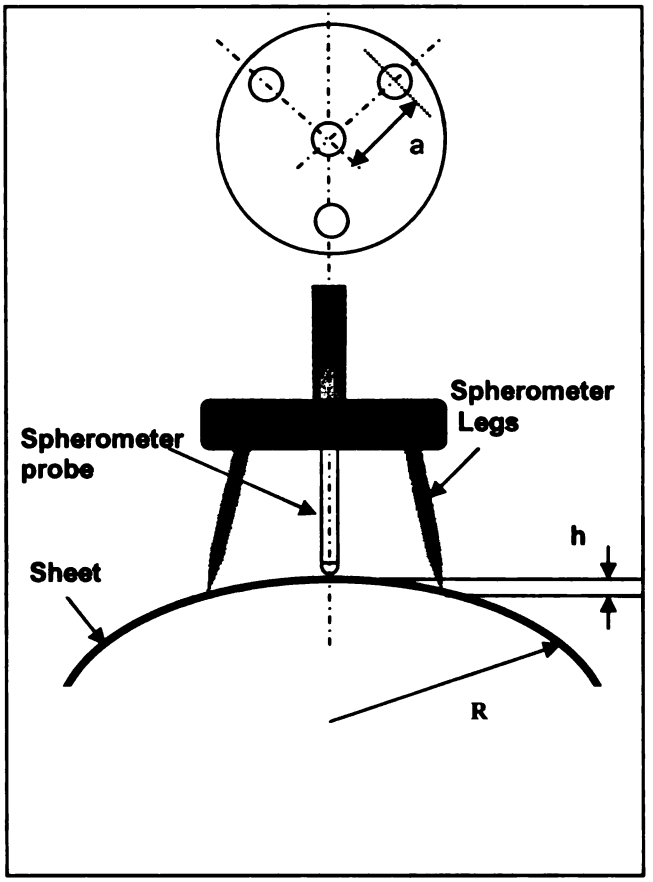

Fig 1.3 shows the schematic of the spherometer used to measure the radius of curvature

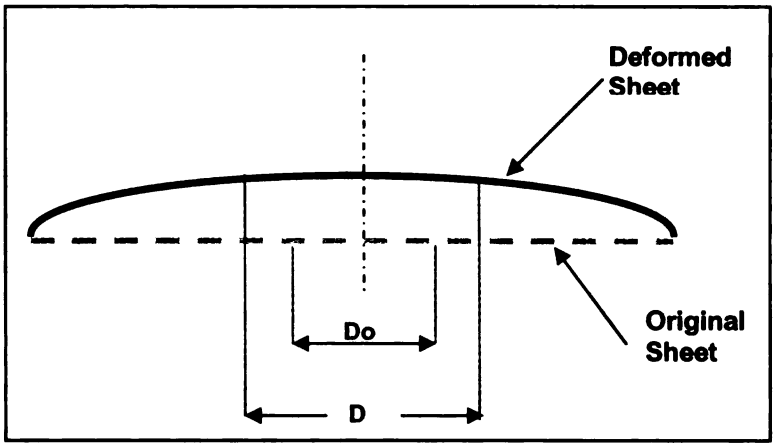

Fig 1.4 shows the change in the chord length 'D' after the deformation of the sheet

The numerical analysis of sheet bulging was performed using the commercial finite element code LS-Dyna. The material model used was the Barlat YLD96 yield function. This material model was previously implemented as a user material (UMAT) subroutine into LS-Dyna code by Abedrabbo [9].

A detailed description of the experimental work carried out is given in chapter 3, and a detailed description of the numerical work done is given in chapter 4. The results from the experimental and numerical work are presented in chapter 5. The conclusions and the scope of the future work is presented after the Results and Discussion chapter. The next chapter gives a brief description of the various literature used in this study.

CHAPTER 2

LITERATURE REVIEW

Much work has been done on the hydraulic bulge testing, almost all work done in this field use similar equipment to measure the stress and strain in a deforming sheet. Regarding numerical work however very little work has been done so far. In this chapter a review of the most recent and significant literature conducted on Experimental and Numerical work for hydraulic bulge testing is presented.

Duncan et al. [1] describe the theoretical basis of the test and the development of equipment necessary to carry out the test. An explanation of why the biaxial test is a much better estimate of material performance than the uniaxial tensile test for certain materials is given. Although stamping with a rigid punch may also simulate biaxial deformation, the results do not match that of the Hydraulic bulge test because friction affects the material behavior. A brief description of the extensometer and spherometer used in the Hydraulic bulge test was given previously along with relevant equations for stress and strain. Also it was stated that for an anisotropic sheet metal measurement of strains along two orthogonal directions (ε_x and ε_y) is necessary since the biaxial deformation at the pole will not be uniform. In the remainder of this thesis the main areas in which the bulge test may be used are outlined and some practical examples of its use are given.

Atkinson [3] describes in his paper the importance of careful attention to detail and precise instrumentation necessary to obtain the desired results. A comprehensive description of the equipment used in his experiment is given and an emphasis on the weight acting on the specimen is presented. To reduce the weight acting on the specimen the extensometer and the spherometer were suspended by light weight pulleys balanced by an equivalent weight. In this thesis it is shown that by applying fluid pressure at a constant rate has the tendency to exponentially increase polar strain rate. A fairly elaborate pressure control process was needed to ensure the required constancy of the strain rate at the pole.

It is also pointed out in this thesis that there is a difference in the initial flow stress between the uniaxial and Biaxial tests. In bulging, the flow stress is initially lower, which is associated with the relatively large contribution of bending to the formation of the bulge. This condition is indicated by the initial rapid increase in the height of the measured polar segment. Eventually, the constrained deformation in biaxial tension emphasizes the initial high rate of strain hardening.

The ALCOA report [5] gives a description of its experimental setup along with the control algorithm, signal conditioning and data processing system. A comprehensive description of the calibration technique used is also given; .the spherometer and the extensometer are calibrated using a ground surface plate. The highlight of this paper is the error analysis which is done by scribing the

sheet with concentric circles of known diameter and then measuring the diameter of the circles along different angles after the test. Based on this analysis it was concluded that the extensometer measurement must be done at 45 degrees to the sheet rolling direction.

For the Numerical analysis, the importance of using the correct boundary conditions, elements, and material model has been emphasized [6,7,8,9]. Although commercial finite element software offers variety of material models, it may not offer specialized model for a specific material and process. This becomes especially important when the process of forming an anisotropic material requires using heat [7]. Thus a specialized material model must be developed which will incorporate the anisotropic characteristics of the aluminum sheet and will have temperature capability to correctly capture the deformation behavior of the material at elevated temperatures.

The Barlat YLD96 and YLD2000-2d material models are one of the most accurate material models because they simultaneously account for yield stress and R-value directionalities [7]. In [8,9], the modified power law flow stress was evaluated as a function of temperature and the effect of temperature on the yield surface and on the plastic anisotropy parameters R_0, R_{45}, R_{90} were studied. Several fitting functions were compared for the anisotropic coefficients of the yield stress and the flow stress.

CHAPTER 3

EXPERIMENTAL WORK

3.1 Experimental Apparatus

The equipment for the sheet bulging experiments was built on an existing Interlaken 75 double action servo press, as shown in Fig. 3.1, manufactured by Interlaken Technology Corporation, Eden Prairie, Minnesota. This Servo press has been used previously by Michigan State University (MSU) students to conduct various experiments such as sheet metal forming, sheet hydroforming, forming of composite sheets, etc. The double action refers to the independent movement of the punch and the clamping mechanism. Although the punch does not play any role in the sheet bulging process, the clamping mechanism is a vital part of the process.

Fig 3.1 The Interlaken 75 Double action servo press manufactured by Interlaken Technology Corporation, Eden Prairie, MN

As mentioned before several modifications were made to the original Interlaken Servo press by previous MSU students Nader Abedrabbo [6] and Mike Zampaloni [14]. The servo press is powered by a hydraulic motor and a pump which is activated and controlled independently from the computer by using the Galil Software provided by Interlaken Technologies. The power unit also powers a Tube Hydroforming machine manufactured by the same company and currently available in the lab.

One of the key components of the experimental setup is the ER3000 pressure controller manufactured by Tescom Corportion, Elk River, Minnesota. The operation of the pressure controller is similar to a hydraulic servo valve but operates on 0-100psi air pressure supplied in the lab. The controller can be interfaced to the computer for accurate control of the pressure using a RS485, 1-5V or 0-20mA signal source. In this case however a RS 485 connection is used. One other important equipment used is the air operated piston pump manufactured by High Pressure Corporation, Erie, Pennsylvania. The pump operates on a 100Psi air pressure. This pump supplies the hydraulic pressure required for the sheet bulging and the ER3000 pressure controller is used to control the pressure according to set-points output by the computer and information received from the external pressure transducer. However through experience it was noticed that for a smooth pressure profile it was necessary to fit a Hydraulic accumulator between the pump and the ER3000, the pump first recharges the accumulator to 3000psi and then the test is completely run from

the accumulator. Figure 3.2 shows the schematic diagram of the overall sheet bulging process with all the vital hydraulics and components. Materials investigated in this research were AA3003-H111, AA5754-O and AA5182-T4, which were supplied by GM. Each test specimen had a dimension of 1mm thickness and a diameter of 6-inches. Table 3.1 shows the mechanical properties of the different materials tested.

Material	Elastic Modulus(GPa)	Poisson Ratio	Yield Strength(Mpa)	Tensile strength(Mpa)
AA3003-H111	70-80	0.33	125	130
AA5182-T4	70-80	0.33	395	420
AA5754-O	70-80	0.33	160	180

Table 3.1 shows the properties of the different alloys of aluminum used for this study.

The major alloying content in the AA3003 material is manganese whereas the major alloying content in the 5754 and the 5182 material is magnesium. The 3003 material is non-heat treatable, has good formability characteristics and corrosion resistance and is used for automotive paneling and surfaces exposed to atmosphere. The 5182 material is non-heat treatable, has very good corrosion resistance and is widely applied for cryogenic use, ship building and structural work. The 5754 material is non-heat treatable and has high temperature resistance, good corrosion resistance and is used for transportation of ammonium nitrate, petroleum, etc.

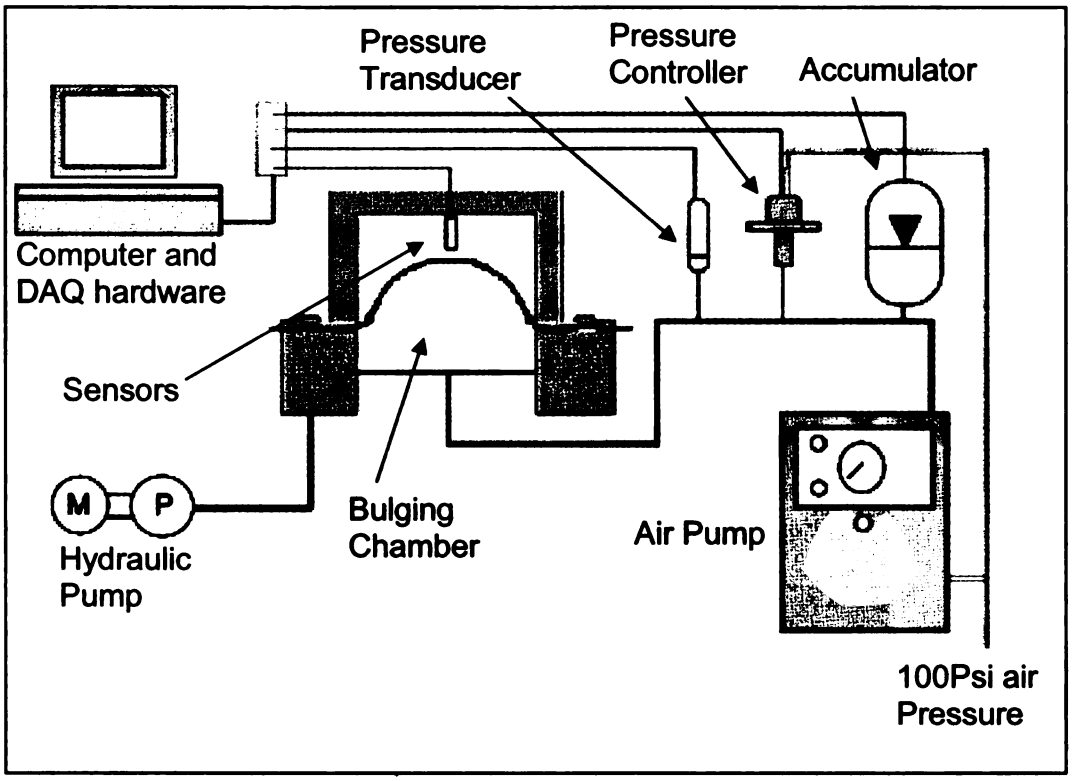

Fig 3.2 shows the schematic of the Sheet Bulging Process with all Vital Hydraulics and Components

The pressure accumulator, shown in Fig. 3.3, serves two important functions and is a very important part of any hydraulic system. In this system it is used for the following two important functions:

- To smooth out the piston pulsations produced by the air operated pump and to provide a smooth pressure profile which is very important to get accurate results.
- To save the system from high pressure surges and to prevent air from entering the pump.

At first the system was operated without the hydraulic accumulator and the piston pulsations were clearly affecting all measurements, therefore resulting in poor data. Once the 1 gallon capacity accumulator, precharged to 3000psi, was added to the system the pulsations were totally eliminated and a smooth pressure profile was obtained, as shown in Fig. 3.4.

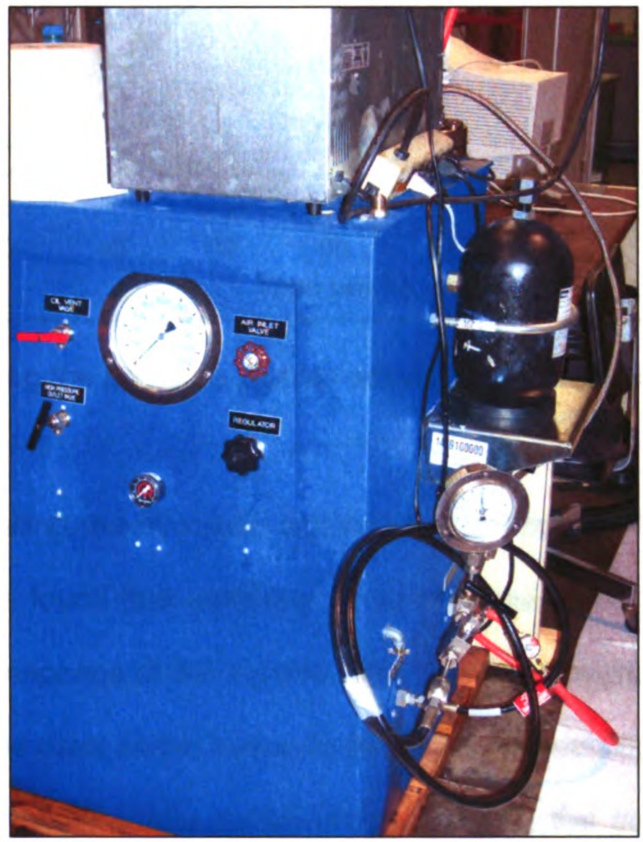

Fig 3.3 Shows the Air operated pump and the hydraulic accumulator used.

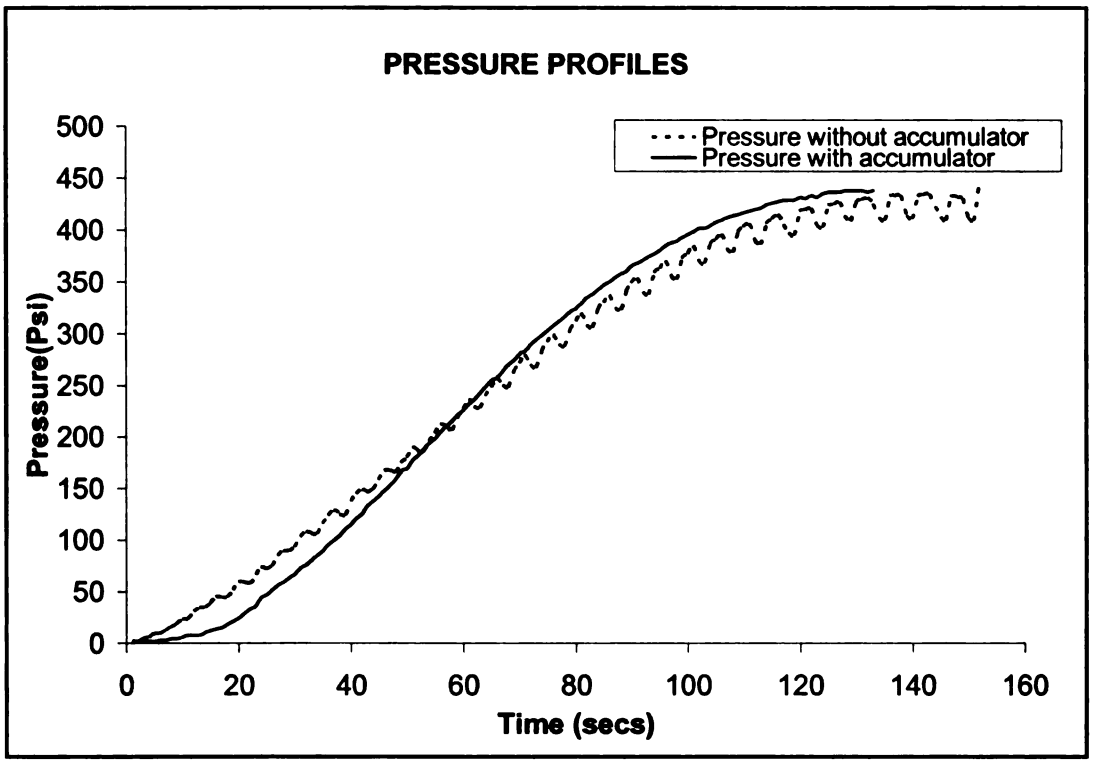

Fig 3.4 showing the pressure profiles without and with the accumulator

Apart from incorporating the hydraulic accumulator to improve the performance of the system, it was found that replacing water with peanut oil as the hydraulic fluid increased the response of the system. Also since the peanut oil has a high boiling point, it can be used as the hydraulic fluid when conducting similar tests at elevated temperatures. The only disadvantage in using the peanut oil versus water is that it is messy and difficult to clean and more expensive than water to store and maintain.

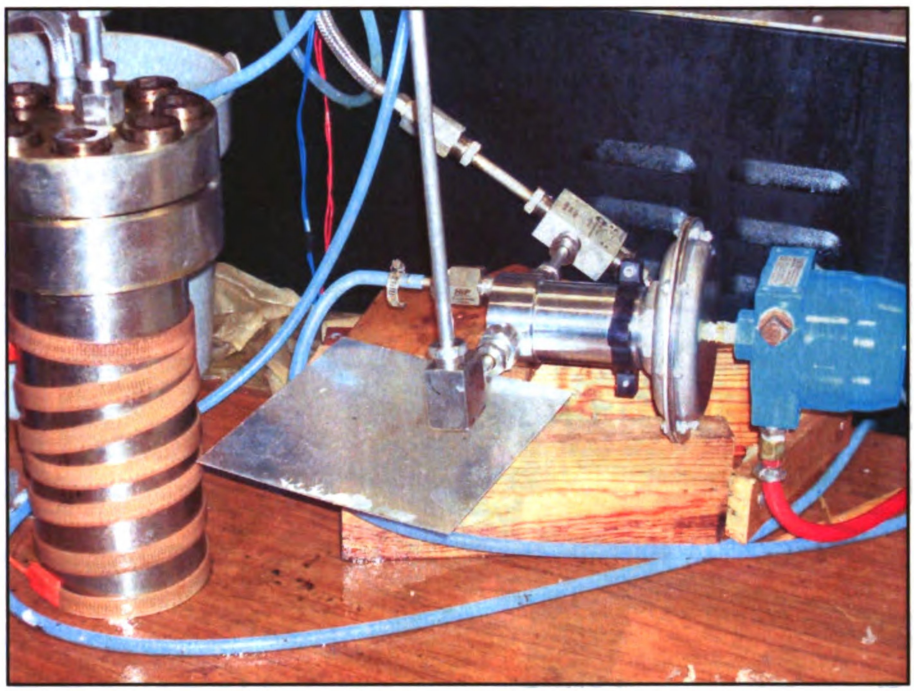

Fig 3.5 the ER3000 Pressure controller and the pressure vessel used for the sheet bulging

A pressure vessel which does not really play an important role in this study is currently connected between the air operated pump and the pressure controller. As shown in Fig 3.5 a flexible heating coil is wound around the pressure vessel in order to heat the hydraulic fluid for when the sheet bulging test must be conducted at elevated temperatures. Pressurized fluid can be stored in the pressure vessel and then heated to the desired temperature before the test is being conducted. It is to be noted that all components of the hydraulic system used in this study are rated to sustain a maximum pressure of 3000Psi and all equipment except the miniature LVDT (explained later in this chapter) can sustain temperatures of up to 500F. Figure 3.6 below shows the Interlaken Servo press with the sheet and sensors connected to the data acquisition system on the computer.

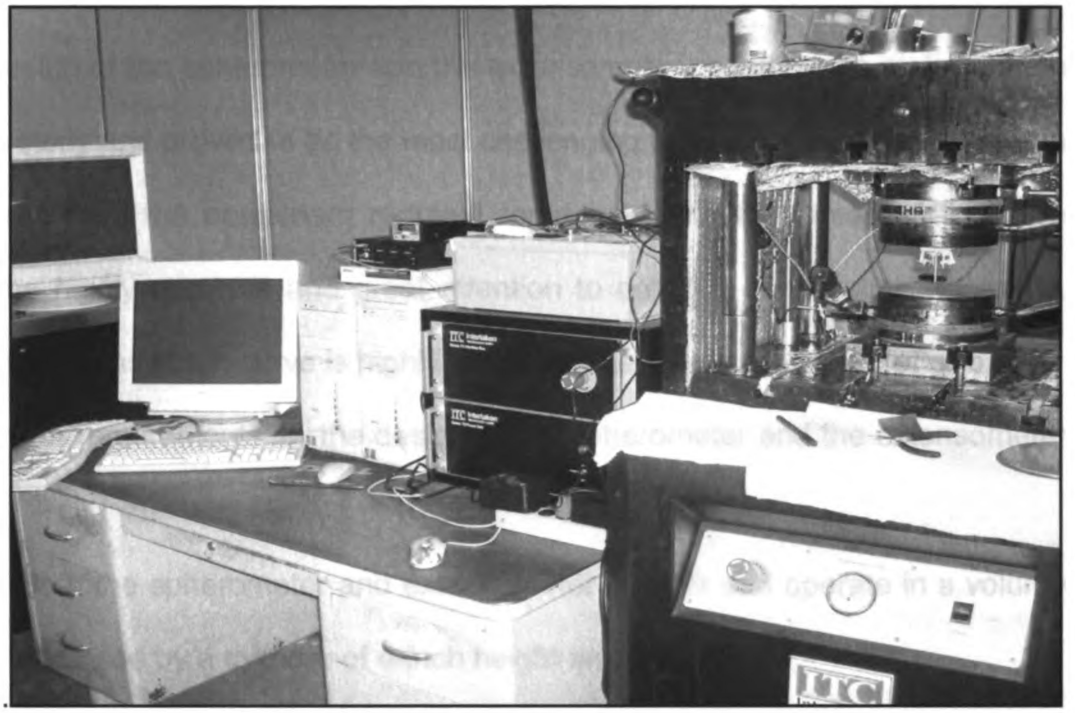

Fig 3.6 shows the Interlaken Servo press with the sheet and sensors connected to the data acquisition system on the computer

All sensors are connected with a 'National instruments' terminal block SCB-68 which in turn is connected to the computer through a 'National Instruments' Ni-6024E multifunction data acquisition card. One of the important requirements of this test is that the data acquisition system must be highly accurate and must have a high sampling rate. This card is capable of a high sampling rate of 250Ksamples/sec and hence is a good choice for this application. The software used for data acquisition and control is National Instruments, Labview 7.0 Express. The choice of this software again proved to be a good one because it not only reduced the lead-time for learning and implementation of the code but also proved to be very reliable and highly accurate.

3.2 Design of Spherometer and Extensometer

The design of the spherometer and the extensometer constitutes a major portion of this study and proved to be the most challenging task. According to pioneers in this area [1,5] the equipment required for determining the stress strain curve must be highly accurate and great attention to detail is an absolute necessity, since the stress strain curve is highly sensitive to even small amount of errors. The major requirements for the design of the spherometer and the extensometer are:

- Both the spherometer and extensometer must fit and operate in a volume enclosed by a cylinder of 4-inch height and diameter.
- The moving and sliding parts of the equipment must operate with a very small amount of force and must not influence the deformation of the specimen.
- The equipment must be as light as possible and must not influence the deformation of the specimen.
- It must be highly sensitive to record small changes in strain.
- The equipment must be water and oil resistant and must be able to withstand the high pressure splash caused when the sheet cracks.
- It must be temperature resistant up to 500F when the test is being conducted at elevated temperatures, and must be able to give accurate results even at high temperatures.
- The equipment must have linearity in the output signal and must be easy to interface with the computer.

The design of the spherometer proved to be pretty straight forward and required little design changes once the first prototype was built. As shown in Fig. 1.3 it consists of a vertical LVDT with its probe touching the sheet, and a tripod is connected to the bottom of the LVDT which rests on the sheet. The body of the LVDT slides in a small channel within the frame of the Interlaken servo press. As the sheet deforms the probe moves upward and measures the distance 'h' as shown in Fig. 1.3.

The design of the extensometer proved to be more challenging because it involved more contact with the sheet and also because it had more moving parts, which influences the accuracy of measurement. The final successful design is a product of two earlier prototypes which used different measurement techniques but failed to satisfy all of the design requirements.

3.2.1 Prototype 1 – Use of Strain Gages.

Foil resistance strain gages have long been used as a means to measure the strain in a specimen. It is a known fact that strain gages can measure as small as one μ-strain. Hence in terms of sensitivity of measurement a strain gage is a good choice for this application. To increase the accuracy of the measurement two strain gages were used, the design is shown in Fig. 3.7. The strain gages are bonded onto either side of a flat strip of spring steel. This strip acts as a spring and is bent so that it can be glued onto the surface of the aluminum sheet.

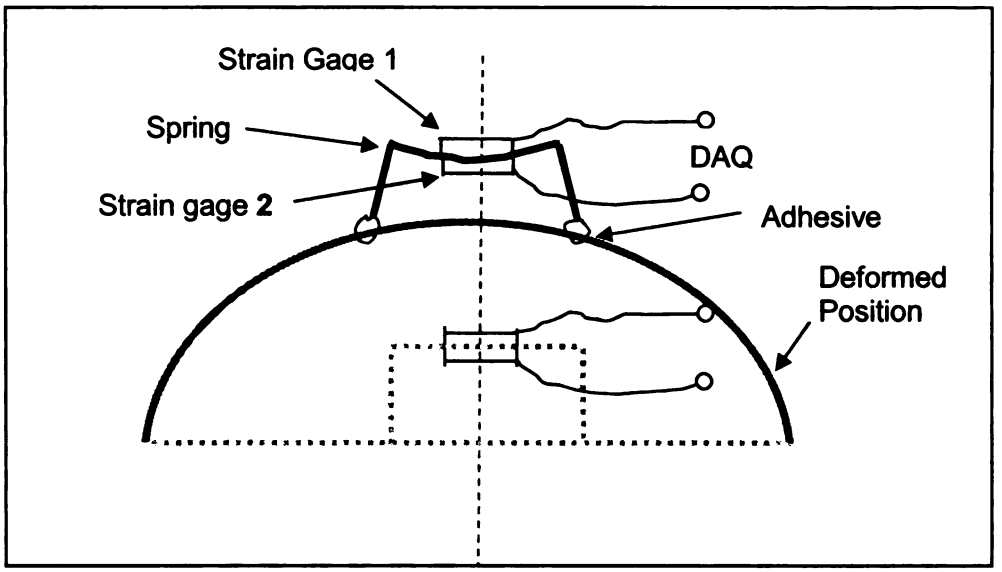

Fig 3.7 shows the use of strain gages as a means to measure the true strain

One strain gage measures the compression on the spring and the other (bottom) strain gage measures the tension, the result of the two strain gages is averaged and an accurate measure of the strain is obtained. The ends of the two strain gages are connected to a 'National instruments' NI-SC-2345 signal conditioning accessory. The ends are connected to a strain gage module which fits in the signal conditioner.

Before the spring is mounted on the specimen, it needs to be calibrated. Calibration is done by mounting the two legs of the spring on the legs of a vernier caliper and the legs are moved at a known distance and the corresponding voltage reading from the strain gages is measured. In this manner the legs of the vernier are moved for several known voltages and the corresponding voltages are recorded. With these results at hand, a graph of voltage versus distance is

obtained which is implemented in to a Labview code as a result of which we obtain real time measurements of strain as the specimen is being deformed.

However there is a major problem associated with this type of setup and that is with bonding between the spring and the aluminum specimen. Various techniques were used to create a flawless bond between the spring and the sheet, but none proved effective. Initially a high temperature thermoset adhesive was used, which formed a rigid bond upon heating it to 200F. Due to the rigidity of the bond it would easily crack and loosen the bonding as the specimen was being deformed. So from this experience it became obvious that a flexible bond with the same strength as the previous bond was needed. This seemed to be working well initially but then as the stiffness of the spring increased the bond became highly tensile and would result in wrong strain measurements. Soldering or welding seemed to be good options at this point but there were no good soldering techniques available to bond a spring steel sheet to an aluminum sheet. Welding would result in melting the aluminum sheet, which will again affect the deformation characteristics of the sheet and would result in incorrect readings. Also it was noticed that considerable amount of force was necessary to elastically expand the spring with the two strain gages bonded to it.

So it was concluded that though the use of strain gages seemed to be a good option in terms of sensitivity and accuracy, the lack of effective bonding

techniques between spring steel and the deforming aluminum sheet resulted in a total rejection of this technique to measure strain.

3.2.2 Prototype 2- Use of LVDT and a Single Extensometer Leg

Since the use of strain gages failed to satisfy our need, the next step was to redesign the extensometer with the use of an LVDT and a lever mechanism to measure the strain of the specimen. While it is pretty straight forward to design a link with hinge system to detect the change in strain, the challenging part was to find a suitable LVDT which is small enough to fit inside a cylinder of 4 inches height and diameter. A miniature LVDT manufactured by Microstrain, Inc, Williston, Vermont served our purpose. The miniature LVDT, shown in Fig. 3.8, which has a body length of 25mm and diameter of 2mm proved to be an excellent candidate for this application. Table 3.1 below shows the specifications for the miniature LVDT used for the design of the extensometer.

Stroke	9mm
Sensitivity	2volts/mm
Resolution	0.06 microns
Temperature Resistance	220 Celsius for 10 mins

Table 3.2 specifications for the Microminiature LVDT used for the Extensometer

While the resolution of the LVDT seemed to be adequate for this application it was found that the sensitivity of the system had to be increased by external amplification (use of levers) in order to measure the very small change in strain at the start of the experiment.

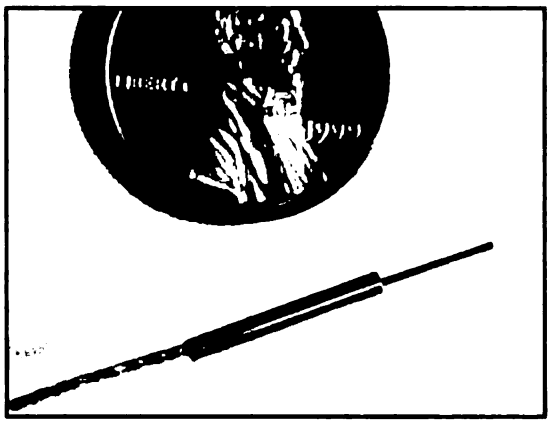

Fig 3.8 shows the Micro miniature LVDT used for the Extensometer

The LVDT has a high temperature resistant cord which can withstand temperatures of 300C (572F), and the LVDT itself can withstand temperatures up to 220C (428F) and hence is suited for the high temperature application. The LVDT is connected to a Smart motherboard supplied by Microstrain, Inc., which converts the analog signals to suitable digital signals read by the computer. The LVDT is housed inside the housing on the extensometer and the probe of the LVDT is hinged onto the lever of the extensometer leg as shown in Fig. 3.9.

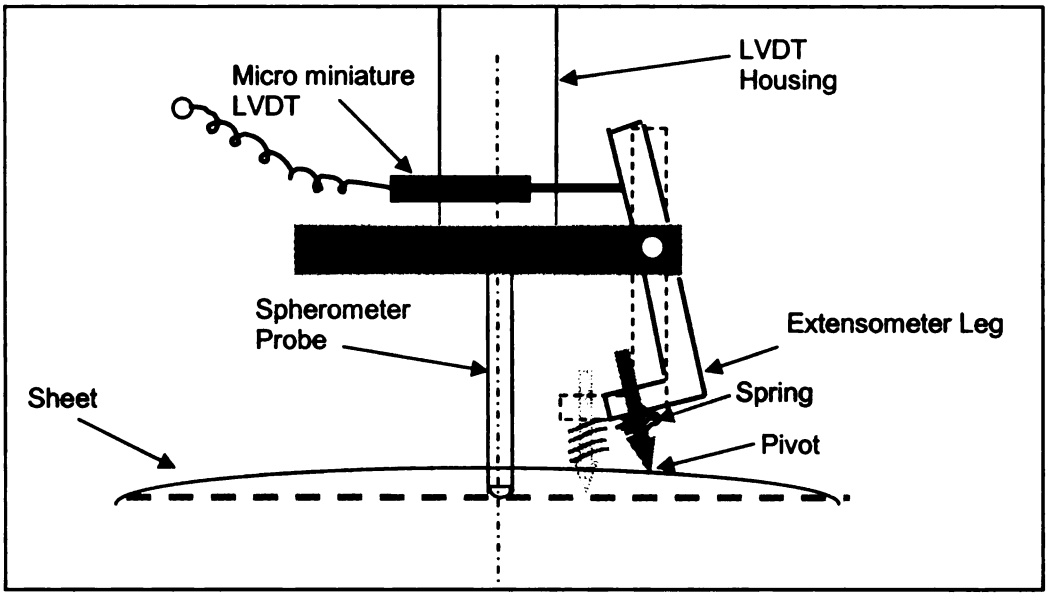

Fig 3.9 shows the schematic of the prototype of extensometer using a miniature LVDT and a single extensometer leg.

As the name suggests this extensometer design uses a single leg, which is based on the assumption that as long as the measurements are taken within the uniform biaxial region, any measurement from the center of the bulge to a point within the biaxial region is constant for all points lying in the same radius. Thus measurement is taken using only a single extensometer leg and then multiplied by a factor of two to get the total measurement. This design is simple and can easily accommodate the LVDT with its housing and hinge.

The leg has a spring loaded pivot which rests on the sheet, this spring is necessary to facilitate the upward movement of the sheet as it is being deformed. The end of the pivot which rests on the sheet is machined down to a point. Initially it was anticipated that the sharp pivot will dent the sheet and will fit in the dent as the sheet is being deformed. But it was found that as the curvature of the

sheet increases the sharp pivot pierced into the sheet resulting in premature failure of the sheet.

A sheet with a premature failure has a much lesser bulge height than a sheet that fails normally and hence it was concluded that though increasing the sharpness of the pivot resulted in a good contact between the sheet and the pivot it resulted in premature failure of the sheet which gives wrong results. Fig 3.10 shows the comparison in bugle height between a sheet under normal failure and a sheet that failed prematurely.

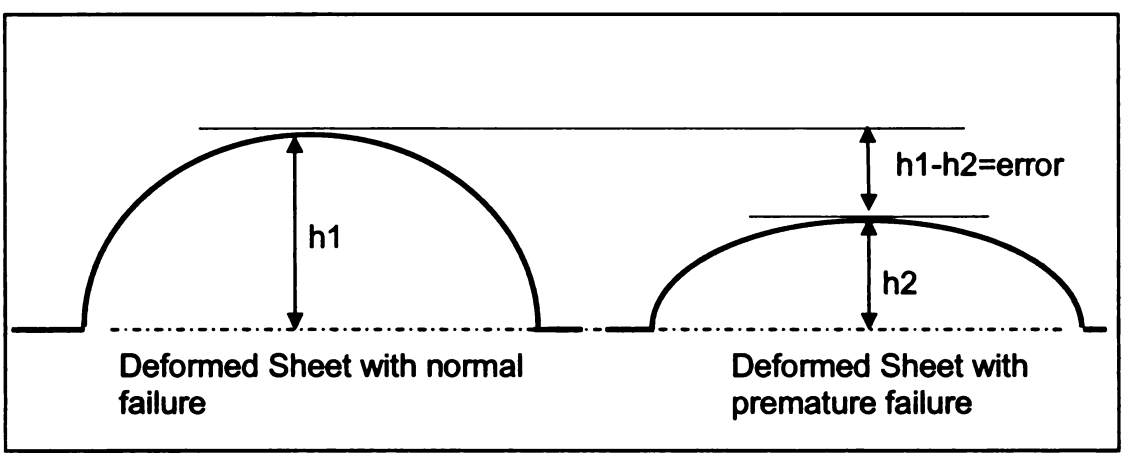

Fig 3.10 shows the difference in bulge heights between a sheet with normal failure and a sheet which has failed prematurely.

In order to prevent the premature failure of the aluminum sheets the sharpness of the pivots was reduced. Reducing the sharpness improved the results because the percentage of premature failure of the specimens reduced drastically, however there was a new problem of 'slipping' between the pivot and the sheet. Slipping is caused when there is lack of friction between the pivot and the sheet and hence the strain is not accurately predicted by the extensometer. To prevent

this slipping the spring stiffness on the pivot was increased, increasing the spring stiffness meant that more weight must be added to the assembly in order to balance the extra spring stiffness.

It was found that increasing the spring stiffness reduced the amount of slip between the pivot and the sheet but the extra weight caused the spherometer legs to pierce into the specimen and still cause premature failure. An attempt was made to find an optimum weight on the equipment which did not cause premature failure and also prevented failure, but it was then realized that in order to cause unconstrained deformation of the specimen there must be minimum or negligible weight on the specimen.

One other problem that was faced with this design is the use of a single extensometer leg, the single leg failed to be sensitive enough to predict the initial small change of strain. The effect of low sensitivity of the extensometer will lead to inaccurate measurement of the strain and this effect is shown in Fig. 5.5 in the Results and Discussion chapter.

Based on all these factors it was concluded that the use of single extensometer leg is not a good option for this application and hence the design must be modified to incorporate two legs, the use of the spring and sharp pivot leads to premature failure of the specimen and must be avoided and lastly there must be negligible weight on the specimen to obtain good results.

3.2.3 Prototype 3 – Use of Two Extensometer Legs

The previous two extensometer designs had the main disadvantages of low sensitivity, problem of slipping and causing premature failure in the sheet. A new design had to be made that overcame all these problems. To overcome the problem of low sensitivity in the previous models two extensometer probes were used. The same microminiature LVDT used in the previous model was again used by mounting it between the 2 probes. Since the premature failure was caused due to the presence of the sharp extensometer probes and the spring force, the usage of the spring was avoided in the new design and a specially designed 'rubber wedge' was inserted at the base of the extensometer probes. The use of the rubber inserts not only prevented premature failure but also avoided the use of complex spring mechanisms, see Fig. 3.11.

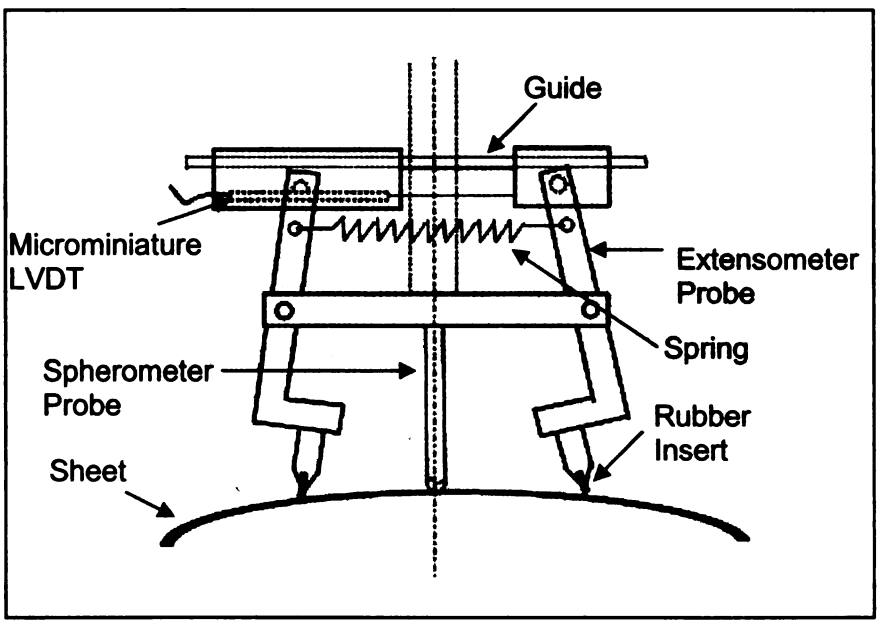

Fig 3.11 shows the schematic of the prototype with two rubber tipped extensometer probes (spherometer not shown)

Each extensometer probe tip is retrofitted with a rubber wedge and held in place by a cylindrical clamp ring. The rubber insert protrudes 0.5mm from the probe tip. The rubber produces the necessary friction between the probe and the deforming sheet. Fig 3.12 below shows the exploded view of the extensometer tip with the rubber insert.

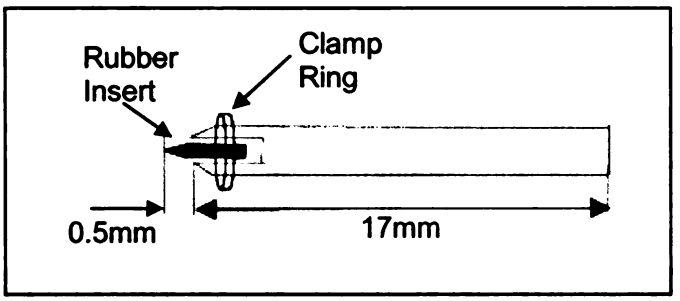

Fig 3.12 shows the exploded view of the extensometer tip with rubber insert

The miniature LVDT is placed inside a block which is hinged to one of the extensometer probes and the core of the LVDT is hinged to the other extensometer probe. A cylindrical rod which acts as a guide slides inside the block to make sure that the LVDT measures the horizontal distance between the extensometer tips. A spring with a small spring constant 'k' is connected between the two extensometer probes, as shown in Fig. 3.13; this spring facilitates easy movement of the probes as the sheet is being deformed. Figure 3.14 shows another view of the extensometer and spherometer placed in position along with the deformed sheet.

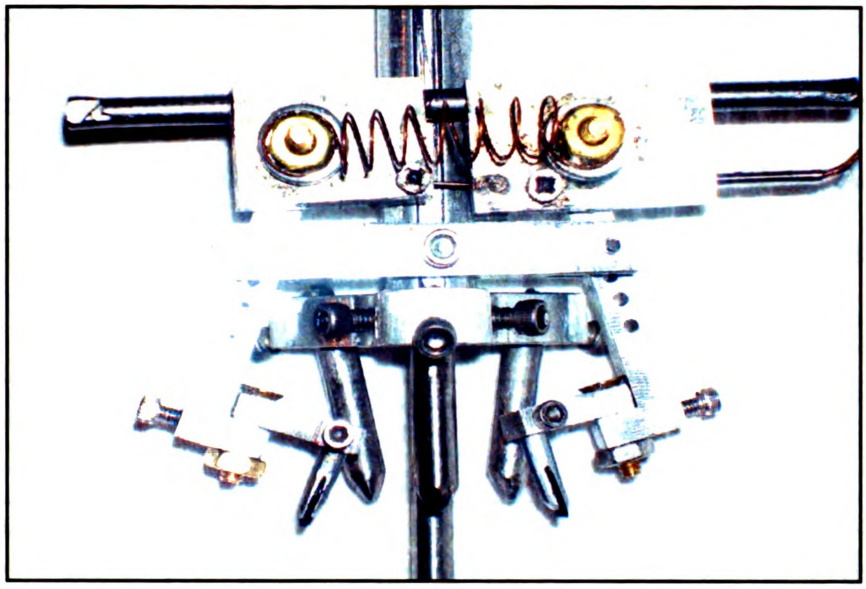

Fig 3.13 shows the Extensometer and Spherometer assembly

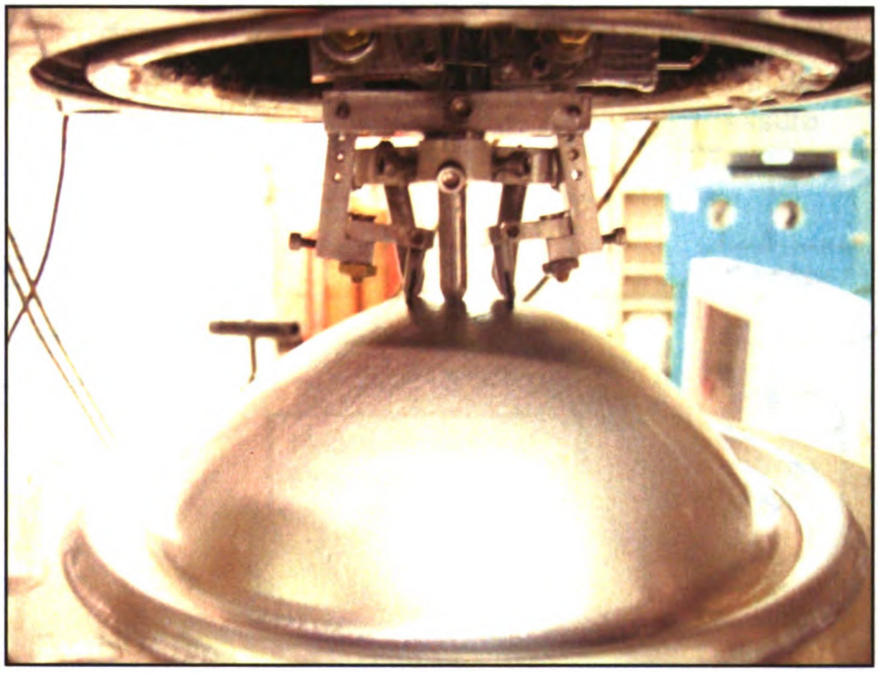

Fig 3.14 shows another view of the Extensometer and Spherometer placed in position along with the deformed sheet

3.3 Strain Rate Control Algorithm

The code for data acquisition, analysis, control and presentation was done using Labview 7.0 express software and National instruments Data Acquisition hardware. The flow chart below, Fig. 3.15, shows the algorithm for the strain rate control.

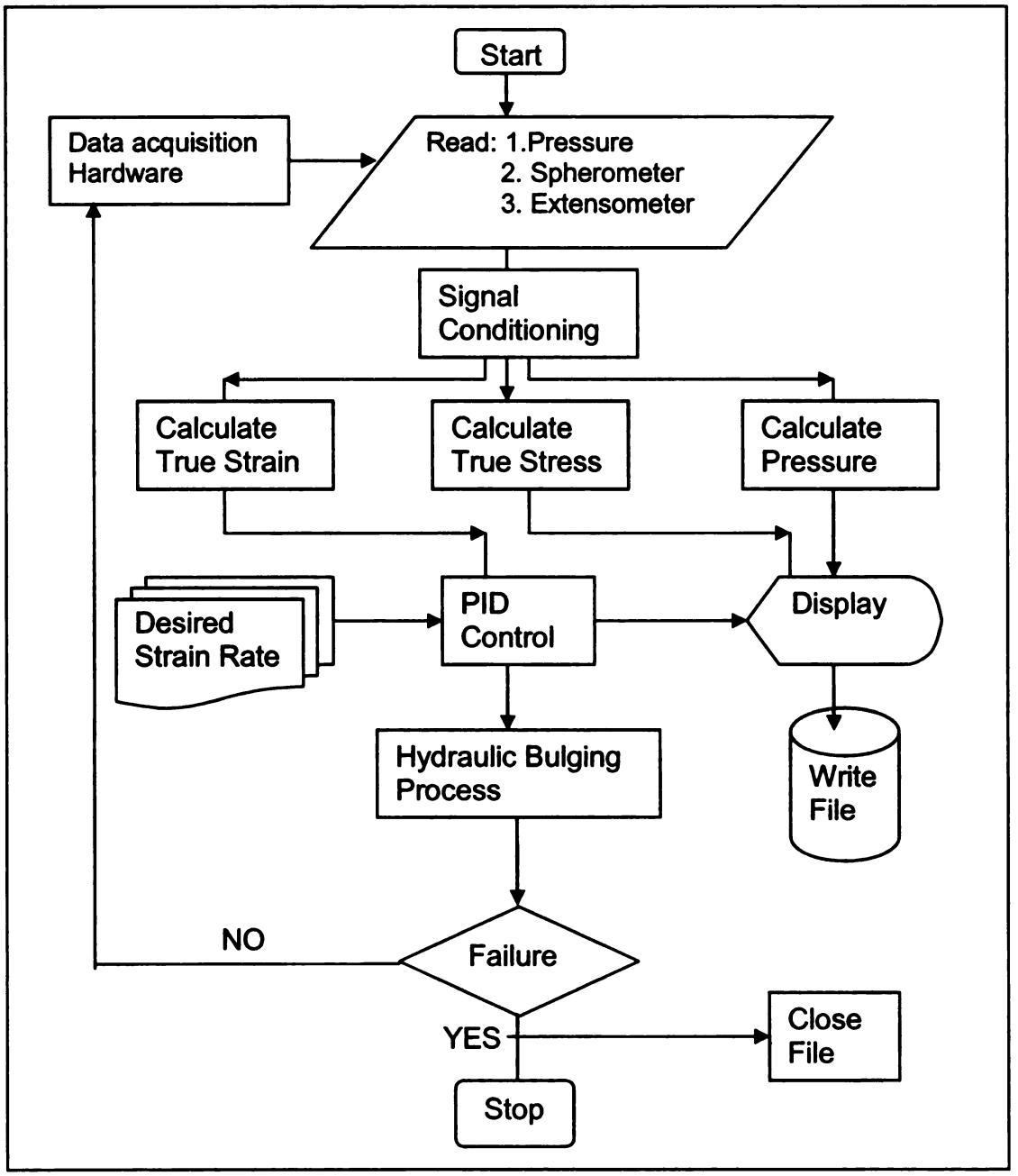

Fig 3.15 shows the Flow Chart for the Strain Rate Control

The Labview software has a graphical programming environment which speeds up the process of developing a code. The data from the three sensors pass through a signal conditioner and then passed to Labview for analysis. The desired strain rate and the calculated strain rate are input to the PID control algorithm. The output of the PID is then fed to the ER3000 pressure controller. All measured and calculated parameters are displayed on the computer screen and sent to a file for subsequent analysis. Once the sheet fails the test is stopped and file is closed. The PID gains are adjusted by trial and error which has to be done only once for a single material, however, the gains may have to be readjusted when testing materials other than aluminum. Fig 3.16 shows the data acquisition and control hardware used in the test.

Fig 3.16 shows the data acquisition and control hardware

Although the strain rate algorithm and the data acquisition system used in the test seemed to work well, it was found that the resolution of the ER3000 pressure controller to control the pressure was insufficient for this application. The outcome of this has been discussed in the Results and Discussion chapter. Table 3.3 shows the comparison of the ALCOA and MSU experimental apparatus for bulge test.

	ALCOA	**MSU**
Blank size	8 inch	4 inch
Pressure controller	Servo valve	ER3000
Control Method	Function generator	Labview / PID
Extensometer	Denting of specimen	Rubber Inserts

Table 3.3 shows the comparison of the ALCOA and MSU experimental Apparatus

3.4 Calibration of Instruments

Because of the inherent nature of the process, the final result is very sensitive to errors and hence accurate calibration of the instruments is an absolute must. The LVDT for the spherometer was calibrated by clamping the body of the LVDT to the table using a C-clamp, and then gage blocks were inserted between the LVDT probe and a fixed reference. The corresponding readings were recorded and then fitted with a linear curve; this function was then input to the labview program. Calibration of the extensometer was done in a similar way except a vernier caliper was used instead of the gage blocks. The Extensometer was fixed on a table in such a way that the extensometer probes were free to move, but the tips of the extensometer probes were fixed by adhesive to the jaws of a vernier caliper. The jaws of the caliper were moved by known displacements and the readings of the miniature LVDT were calibrated against the known readings. Though it is not necessary to calibrate the instruments before every test, it was found advantageous to carry out a calibration procedure after every 3-4 tests. The calibration of the pressure transducer and the ER3000 pressure controller was done by checking the voltage reading on the pressure transducer; for example, at 0 Psi the voltage was checked to be 0V and at 5000 Psi it was checked to be 10V. Using a similar procedure the calibration of the ER3000 pressure controller was checked. The pressure transducer and the ER3000 did not require frequent calibration, unlike the spherometer and extensometer.

3.5 Sequence of Operations

The main steps involved in the sheet hydraulic bulge test are presented in this section.

1. The computer and the data acquisition system is started

2. The air compressor is switched on to supply the 100psi air pressure required to operate the air pump and the ER3000 pressure controller

3. The sheet is placed in the draw bead and the extensometer and the spherometer are placed on the sheet making sure that the extensometer probes are placed at an angle of 45^0 to the sheet rolling direction.

4. Using the Galil software on the computer, the hydraulics is operated and the die is moved up and closed thereby clamping the sheet firmly.

5. The air pump is started and the pressurized fluid is pumped into the hydraulic accumulator.

6. Once the pressure on the accumulator reaches 3000Psi, the air pump is stopped and the test is started

7. The computer program (Labview) is started and the sheet begins to deform based on commands from the computer.

8. The failure of the sheet is noticeable by the sudden drop in pressure in the bulging chamber. At failure the test is stopped and the hydraulic fluid drained from the bulging chamber

9. The die is opened and the deformed sheet is removed and the stored data file on the computer is used for subsequent analysis.

CHAPTER 4

NUMERICAL ANALYSIS

Sheet metal forming is an expensive process because it involves expensive parts such as the die, blank holder, hydraulics and control systems. In addition, there is an expensive design and analysis stage that occurs prior to the actual assembly and manufacturing of parts. For the success of the sheet metal forming process and to reduce the manufacturing cost it is necessary to have a thorough understanding of the sheet metal forming process and various deformation mechanics.

With the advent of finite element method, the cost involved in the design stage can be reduced significantly and with the availability of robust finite element analysis software like Abaqus, LS-Dyna, Ansys, MSC/Nastran, etc the effort involved in modeling and solving the problem has been greatly reduced.

Finite element method can predict failure/defects in aluminum sheets and once the numerical results have been verified with the experimental results they can be used with confidence to predict failure modes for different parameters of the specimen, different material properties, etc. Thus, finite element method is a very powerful tool, provided the complex geometrical contact, boundary conditions and material model are correctly incorporated.

One of the goals of this study were to develop a finite element model of the sheet bulging process at room and elevated temperatures and to compare the numerical results with experimental data to reduce the amount of trial and error involved in the costly and time consuming experimental work.

In this study the numerical analysis was done using the explicit dynamic finite element analysis code LS-Dyna 3D using a user material subroutine (UMAT). The material model used consists of temperature dependent anisotropic parameters which were then implemented as a coupled thermo-mechanical finite element analysis. The material model used was the anisotropic yield function proposed by Barlat et al. (1997a, YLD96). This UMAT was developed by Abedrabbo et al. [8,9] and was used with little modification for this study. The UMAT has been developed for coupled thermo mechanical analysis and hence numerical simulation has been done for room temperature and elevated temperatures for the AA3003-H111 material. Then a comparison of the experimental and numerical results has been done in the Results and Discussion section (chapter 5).

4.1 FEA Code Setup

Ls-Dyna is a general purpose transient dynamic finite element program used for numerical analysis of complex real world problems. Altair Engineering's Hypermesh pre-processor was used to generate the input file for the Ls-Dyna

analysis. Once the input file was generated by Ls-Dyna it was modified outside since Hypermesh does not support all Ls-Dyna cards.

The elements used for the aluminum sheet blank were the 4-node, reduced integration, S4R shell type. Initially, the analysis was carried out using 8-node brick elements (solid elements) but then was changed to the shell elements since there was significant hour-glassing associated with solid elements. The finite element model consisted of 10500 S4R elements and the die and the blank holder were modeled using rigid elements using one integration point through the thickness, as shown in Fig. 4.1.

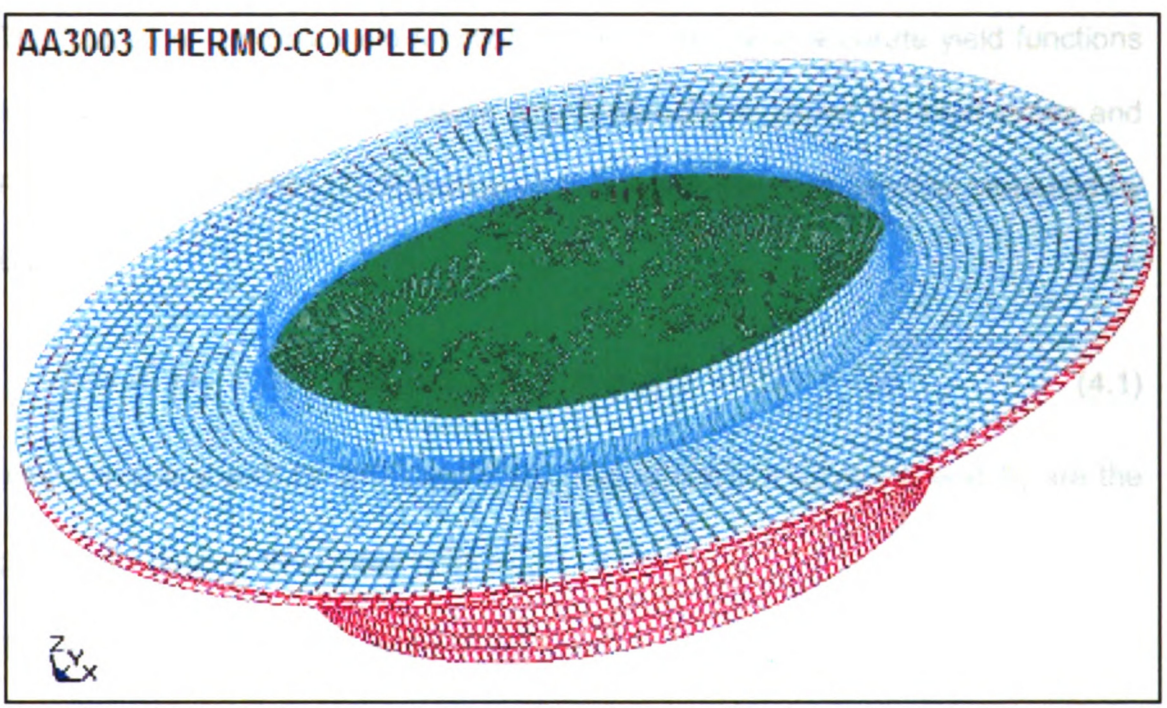

Fig 4.1 shows the numerical model of the die, blank and the blank holder used for the simulation of the hydraulic bulge test

Unlike the experimental setup, which uses a draw bead to grip the blank, the numerical model does not use a draw bead in order to reduce the computation time. By choosing an appropriate friction parameter and a large blank holding

force the sheet was prevented from drawing into the die cavity, therefore creating a pure stretch condition similar to the experiment. A forming limit diagram was also used to predict the onset of failure. The Ls-Dyna has the capability to calculate the FLD using the thickness and the n values of the sheet for steel material. The FLD curves in this research were calculated using the voce-hardening law, which is more accurate than the one used in [6]. As mentioned earlier the UMAT for this numerical analysis was taken from Abedrabbo [9], which was based on Barlat YLD96 material model [21]. Below is a brief description of the YLD96 material model.

The YLD96 anisotropic yield function is one of the most accurate yield functions for aluminum alloy sheets because simultaneously accounts for yield stress and R-value directionalities [7]. Equation (4.1) below is the yield function proposed by Barlat.

$$\Phi = \alpha_1 |S_2 - S_3|^a + \alpha_2 |S_3 - S_1|^a + \alpha_3 |S_1 - S_2|^a = 2\bar{\sigma}^a \qquad (4.1)$$

where a=6 and a=8 for BCC and FCC materials respectively. S_1 and S_2 are the principal values of the stress tensor S_{ij}.

The isotropic plasticity equivalent (IPE) is:

$$S = L\sigma \qquad (4.2)$$

For orthotropic symmetry L is defined using C_k as

$$L_{ij} = \begin{bmatrix} \frac{(C_2+C_3)}{3} & \frac{-C_3}{3} & \frac{-C_2}{3} & 0 & 0 & 0 \\ \frac{-C_3}{3} & \frac{(C_3+C_1)}{3} & \frac{-C_1}{3} & 0 & 0 & 0 \\ \frac{-C2}{3} & \frac{-C_1}{3} & \frac{(C_1+C_2)}{2} & 0 & 0 & 0 \\ 0 & 0 & 0 & C_4 & 0 & 0 \\ 0 & 0 & 0 & 0 & C_5 & 0 \\ 0 & 0 & 0 & 0 & 0 & C_6 \end{bmatrix} \quad (4.3)$$

For the plane stress case ($\sigma_z=\sigma_{yz}=\sigma_{zx}=0$), Eqn. (4.2) reduces to

$$S_{ij} = \begin{bmatrix} Sx \\ Sy \\ Sz \\ Sxy \end{bmatrix} = \begin{bmatrix} \frac{(C_2+C_3)}{3} & \frac{-C_3}{3} & \frac{-C_2}{3} & 0 \\ \frac{-C_3}{3} & \frac{(C_3+C_1)}{3} & \frac{-C_1}{3} & 0 \\ \frac{-C_2}{3} & \frac{-C_1}{3} & \frac{(C_1+C_2)}{3} & 0 \\ 0 & 0 & 0 & C_6 \end{bmatrix} \begin{bmatrix} \sigma x \\ \sigma y \\ 0 \\ \sigma xy \end{bmatrix} \quad (4.4)$$

The principal values of S_{ij} as defined in Eqn. (4.1) are found as:

$$S_{1,2} = \frac{(Sx+Sy)}{2} \pm \sqrt{\left(\left(\frac{(Sx-Sy)}{2}\right)^2 + S^2xy\right)} \quad (4.5)$$

and $S_3=-(S_1+S_2)$ because of the deviatoric nature of S_{ij}. The anisotropy coefficients α_{ij} are defined as

$$\alpha_1 = \alpha_x Cos^2\beta + \alpha_y Sin^2\beta$$
$$\alpha_2 = \alpha^x Sin^2\beta + \alpha_y Cos^2\beta \qquad (4.6)$$
$$\alpha_3 = \alpha_{zo} Cos^2 2\beta + \alpha_{z1} Sin^2 2\beta$$

The constants C_k, where k=1,2,3,6 and α_x, α_y, α_{zo} and α_{z1} are coefficients that represent the anisotropy of the material, the angle 2β, is the polar angle determined from Mohr's circle as

$$2\beta = \tan^{-1}\left(\frac{2Sxy}{Sx - Sy}\right) \qquad (4.7)$$

In order to determine the above coefficients, experimental data was used. Most of the coefficients were obtained from the uniaxial tensile test and some were obtained from the balanced biaxial test. Table 4.1 shows the values of stresses and R-values measured in different directions for each test. These measured properties were then used as input to calculate the anisotropy coefficients of Barlat YLD96 yield function, using the non-linear solver Newton-Raphson with initial values corresponding to the isotropic situation (C_1=C_2=C_3=C_6=1.0).

TEST	**Balanced Biaxial**	**Uniaxial**		
Orientation	N/A	0^0	45^0	90^0
Flow Stress	σ_b	σ_0	σ_{45}	σ_{90}
R - value	N/A	R_0	R_{45}	R_{90}

Table 4.1 gives a summary of the experimental data necessary to calculate the yield function coefficients required for the YLD 96 material model [8]

From the results of the uniaxial tensile tests conducted at different strain rates and different temperatures the values for the Holloman hardening rule (K, n, ε_0, m) were calculated as a function of temperature [8]. Table 4.2 shows these

values for AA3003 material. Table 4.3 shows calculated anisotropy coefficients calculated for AA3003 material.

Temp (°C)	K(Mpa)	n	ε_0	m
25	199.82	0.215	8.3E-04	0.003
38	186.41	0.20	5E-4	0.004
66	175.78	0.187	3.16E-4	0.004
93	168.41	0.179	6.64E-4	0.005
121	146.98	0.175	3.2E-4	0.010
149	139.18	0.163	7.4E-4	0.015
177	119.65	0.157	6.3E4	0.03
204	106.32	0.137	2.31E-4	0.045
232	93.82	0.132	3.71E-4	0.065
260	77.32	0.116	5.05E-4	0.080

Table 4.2 shows the material properties of AA3003 material at elevated temperatures [8]

Temp (°C)	C_1	C_2	C_3	C_6	α_x	α_y	α_{z1}
25	1.1169	0.9545	1.0030	1.0429	0.9130	1.3960	1.250
38	1.1622	1.0424	0.9677	1.0985	0.6516	0.7866	1.040
66	1.2299	1.0232	0.9968	1.0888	0.5038	0.8513	1.156
93	1.2871	1.0478	0.9953	1.0721	0.4810	0.7034	1.508
121	1.0847	1.0171	1.0116	0.9639	0.8060	0.7894	2.110
149	1.1804	1.0318	1.0049	1.0185	0.6182	0.7380	1.806
177	1.1280	1.0619	1.0003	0.9782	0.6650	0.5930	2.146
204	1.1742	1.0681	1.0058	0.9932	0.5382	0.5294	1.901
232	1.2526	1.2095	0.9564	0.9939	0.3160	0.2427	1.969
260	1.2329	1.0994	0.9939	0.9904	0.3920	0.4515	2.123

Table 4.3 shows the Barlat YLD96 anisotropy coefficients calculated at elevated Temperatures

Once all the anisotropy coefficients and the material properties were available the Barlat YLD96 material model was implemented as a UMAT using the cutting plane algorithm proposed by simo et al (1985). A detailed description of the algorithm used in this study is given in [9].

CHAPTER 5

RESULTS AND DISCUSSION

In this chapter the results obtained from the experimental and the numerical analyses have been presented and also a comparison of these results with the experimental results from ALCOA is made. For the experimental results a comparison is made with the ALCOA results for all three different aluminum alloys tested, i.e. AA3003-H111, 5182 and 5754, whereas for the numerical results only the 3003 material is used for the comparison. As mentioned earlier when a linear pressure profile is applied there is an exponential increase in strain, this can be seen in Fig. 5.1 where the original curve obtained experimentally is fitted with a log curve.

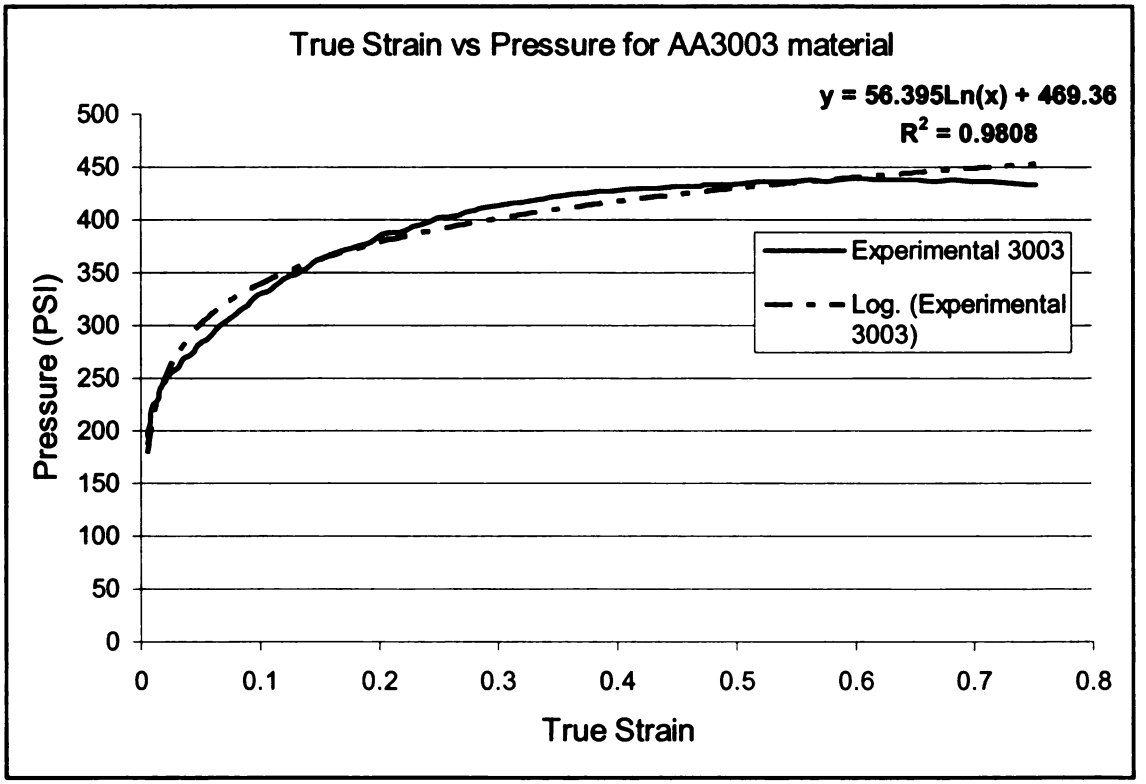

Fig 5.1 shows the experimentally obtained relationship between applied pressure and the true strain

Figure 5.3 shows the bulge test results for the three aluminum alloy sheets tested in this study. This figure is necessary to prove the importance of an external strain rate control system in order to obtain the desired strain rate. ALCOA carried out their experimental tests using equipment designed for a different blank size (8" diameter) than the one used in this study (4" diameter). Though the blank size doesn't affect the final result, this information is provided for the benefit of the reader.

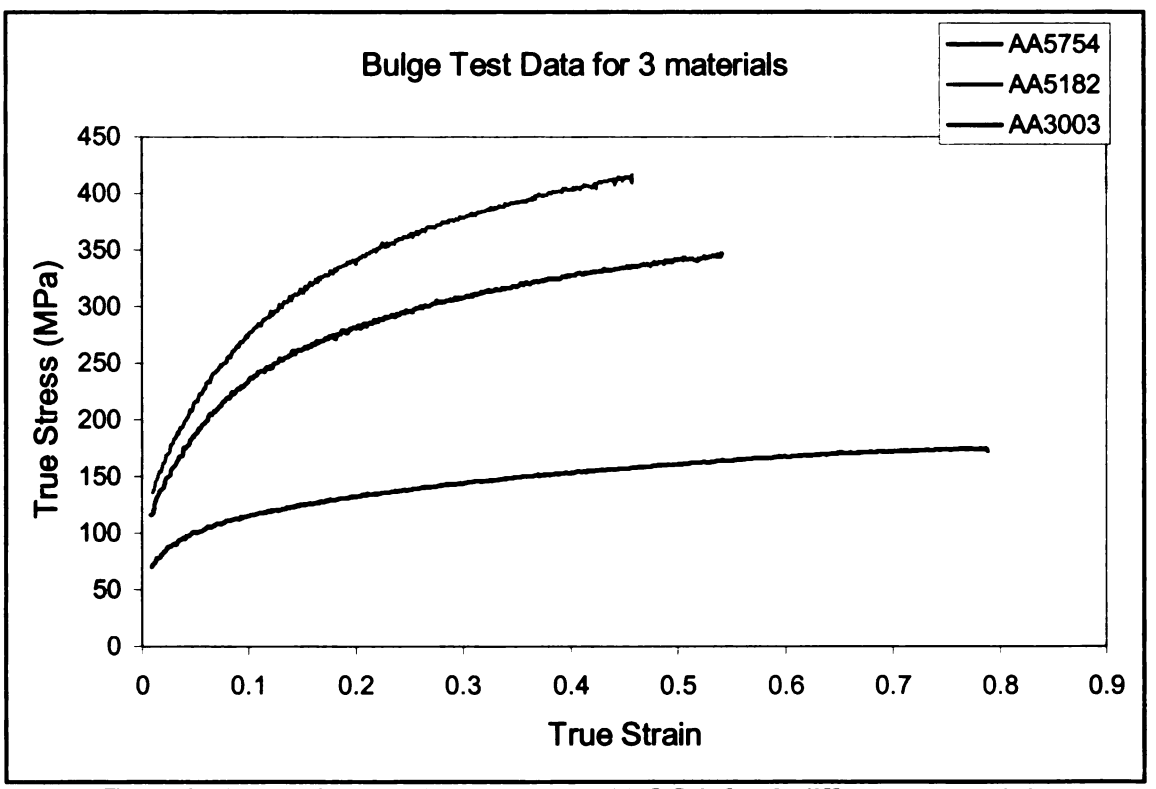

Fig 5.2 shows the results obtain by ALCOA for 3 different materials

5.1 Effect of Premature Failure and Low Sensitivity

In this section the results obtained with the extensometer prototype which incorporated a single probe and a spring is presented. As can be seen from Fig. 5.4, the specimen has failed at a strain of 40% whereas the ALCOA specimen fails at 80% strain. This clearly indicates the premature failure of the specimen due to puncture caused by the sharp extensometer and spherometer probes. Another interesting observation that could be made about the single probe extensometer is its insensitivity at the start of the experiment where the rate of change of strain is very small with respect to stress.

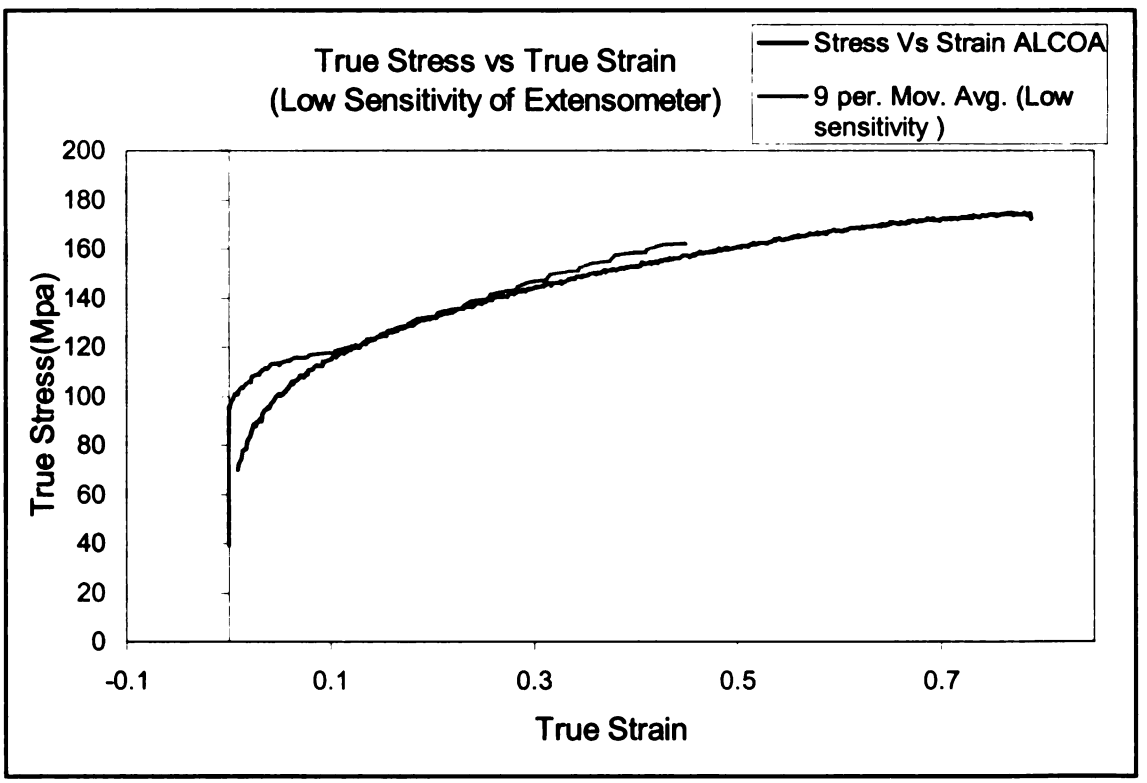

Fig 5.3 shows the effect of insensitivity and premature failure on the specimen

The premature failure of the specimen is also caused due to the addition of the weight on the equipment in order to balance the force produced by the spring on the extensometer probe. The effect of weight on the equipment is discussed in detail in section 5.3.

5.2 Effect of slipping

To prevent the premature failure of the specimen the weight that was applied on the sensor equipment was reduced, this reduced the percentage of premature failures in the specimens but caused problem with 'slipping' between the extensometer probe and the sheet. The effect of slipping can be detected by observing the rate of change of the chord length measured by the extensometer. For a slip-free test the rate of change of the chord length must be smooth whereas for a test with inherent slip the rate of change of the chord length is discontinuous, as shown in Fig. 5.5.

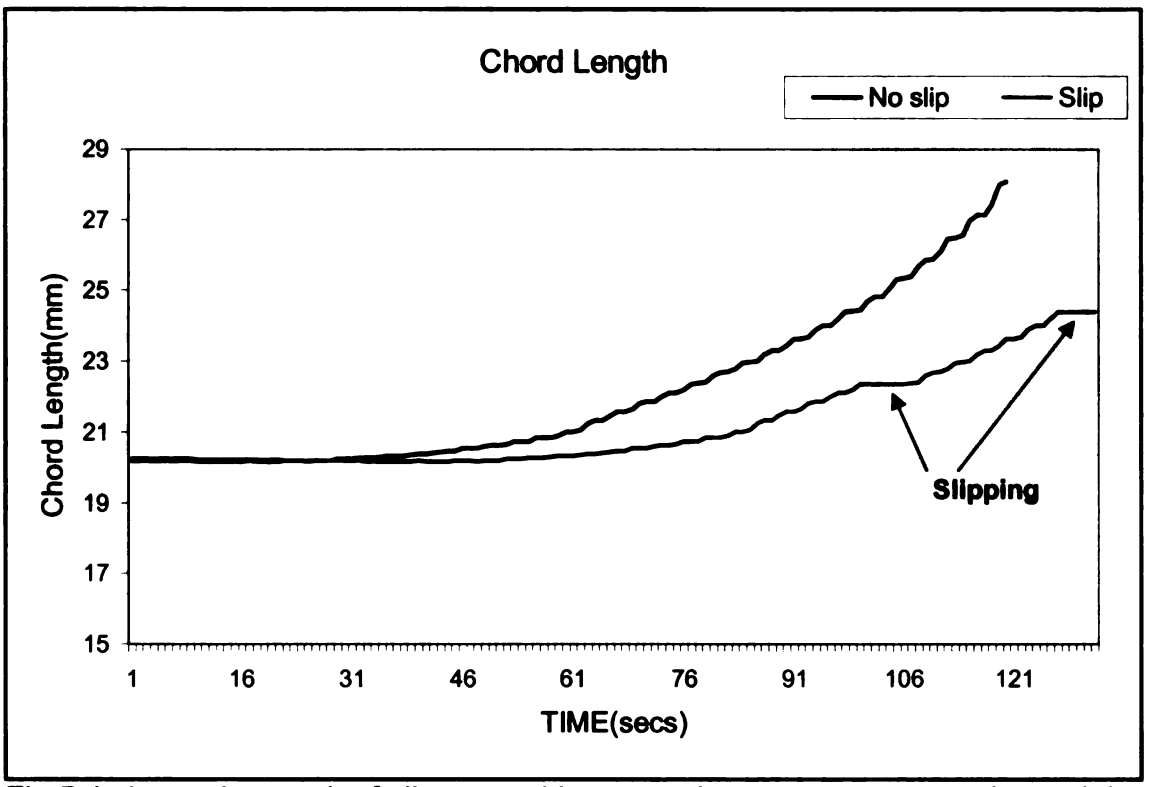

Fig 5.4 shows the result of slip caused between the extensometer probe and the sheet

5.3 Effect of weight on the sheet

As seen from the previous two sections the weight on the spherometer and extensometer was necessary in order to prevent slipping between the extensometer probe and the sheet but the presence of weight caused premature failure in the specimen. This dilemma led to the quest for finding the optimum weight on the sheet that caused negligible slipping and no premature failure. It can be seen from Fig. 5.6 that the addition of the weight causes the stress in the sheet to increase and consequently cause an early failure. It was therefore concluded that for accurate results there must be no weight on the sheet.

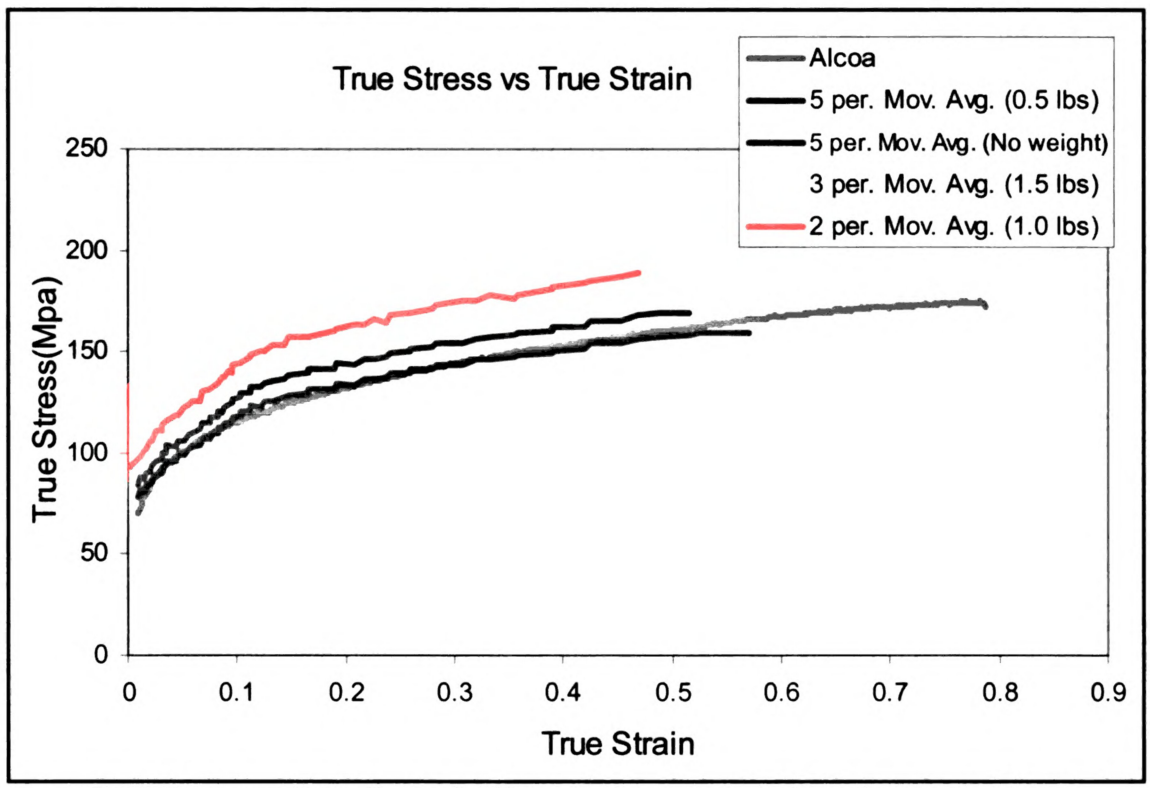

Fig 5.5 shows the effect of different of weights on the aluminum sheet

5.4 Results From Final Prototype

As described in chapter 3, the final prototype was designed to overcome the drawbacks of the first two prototypes. This model uses 2 extensometer probes to increase the sensitivity of the system and has rubber inserts in the probes to increase friction between the probe and the sheet and prevent slipping. The stress vs strain plot obtained from this model is shown in Fig. 5.7 below.

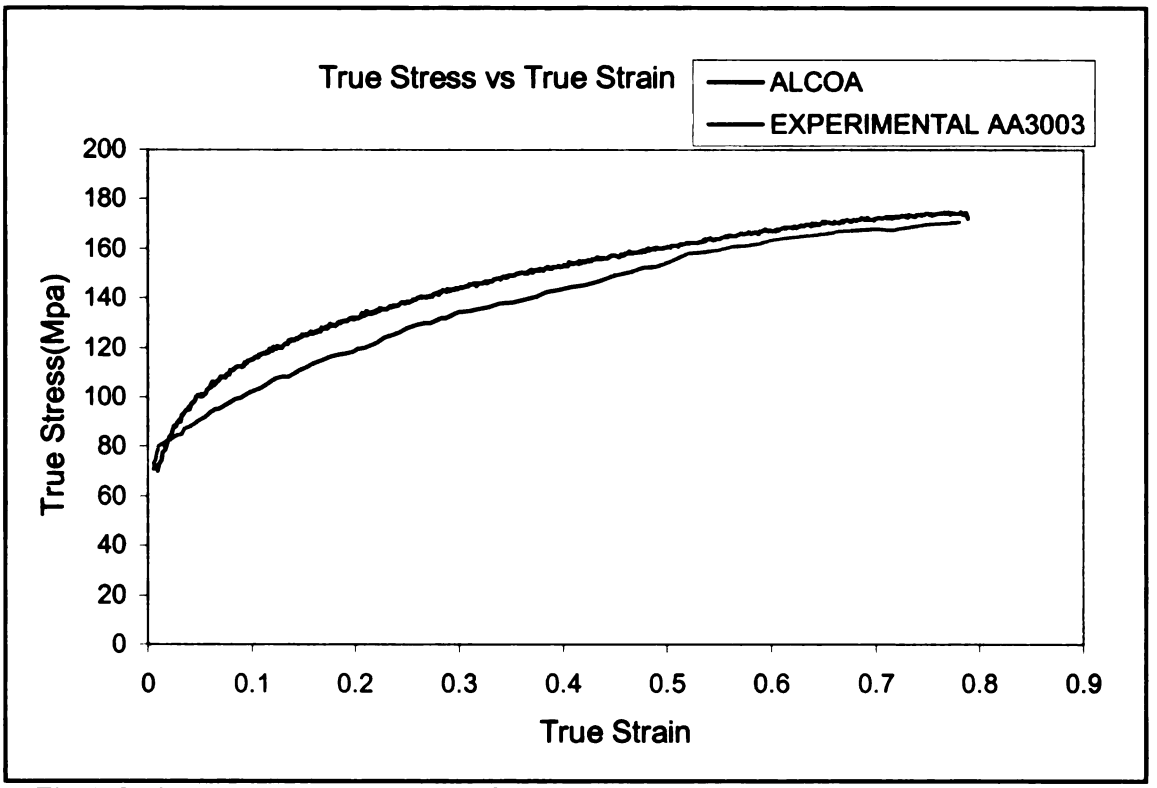

Fig 5.6 shows the comparison of experimentally obtained results for the final prototype

As seen from the above plot there is a good agreement between the experimental result and the result obtained by ALCOA, the slight discrepancy in the result could be due to material hardening. Fig 5.8 shows the results obtained for two other results AA5182 and AA5754 and the comparison with Alcoa's result.

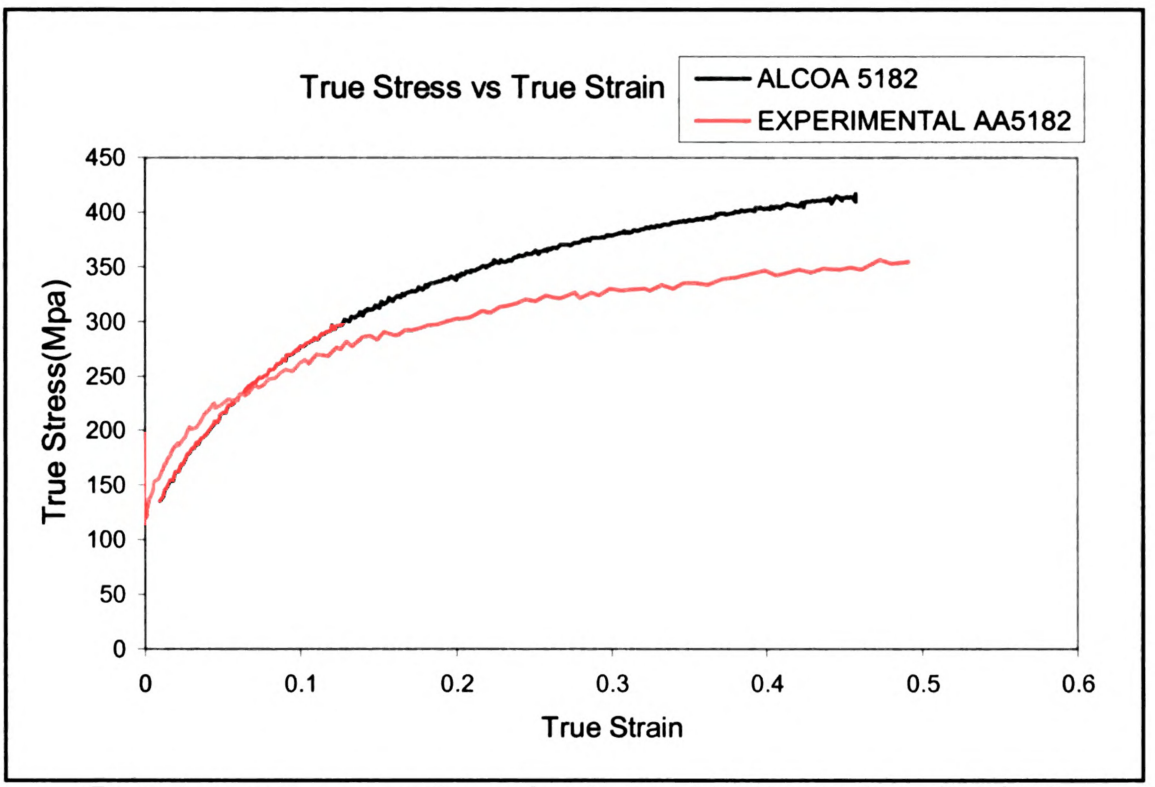

Fig 5.7 gives the comparison of material AA5182 with that of ALCOA

Fig 5.8 gives the comparison of material AA5754 with that of ALCOA

5.5 Numerical Results

This section gives the comparison between the Numerical results, Experimental results and the ALCOA results at room temperature, Fig. 5.10.

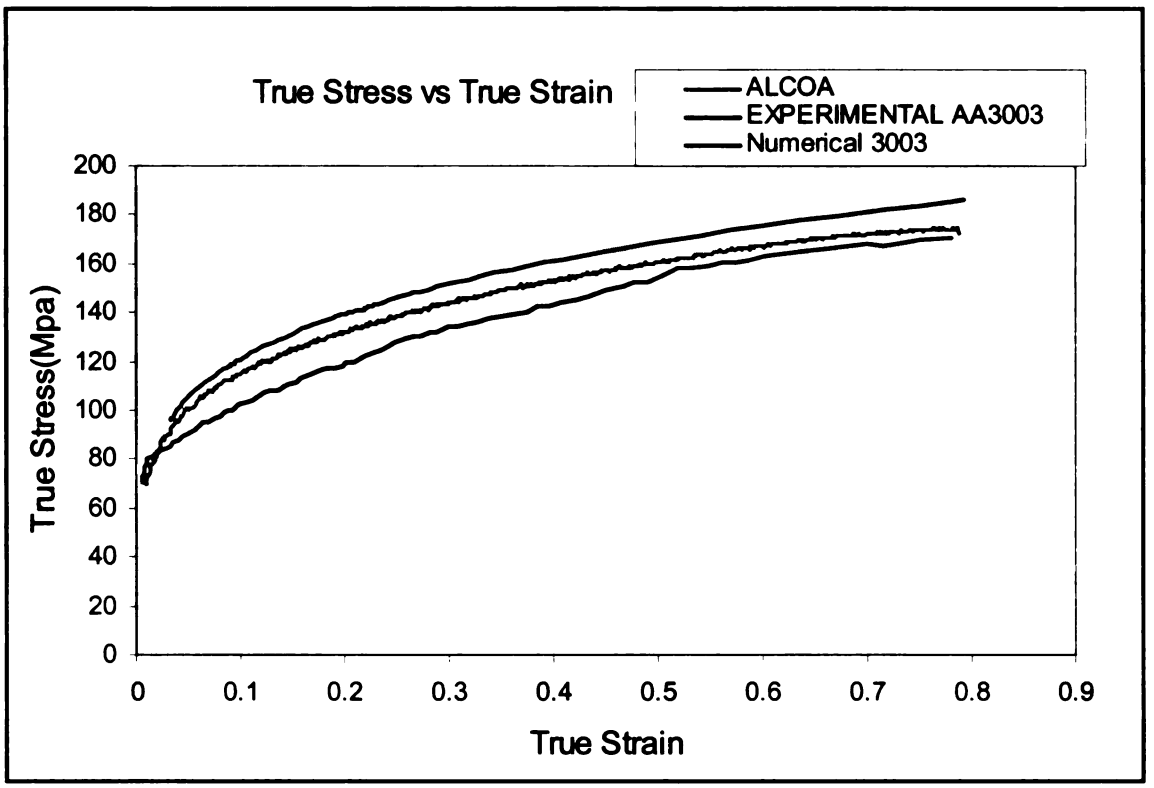

Fig 5.9 shows the comparison graph between the Numerical, Experimental and the ALCOA result

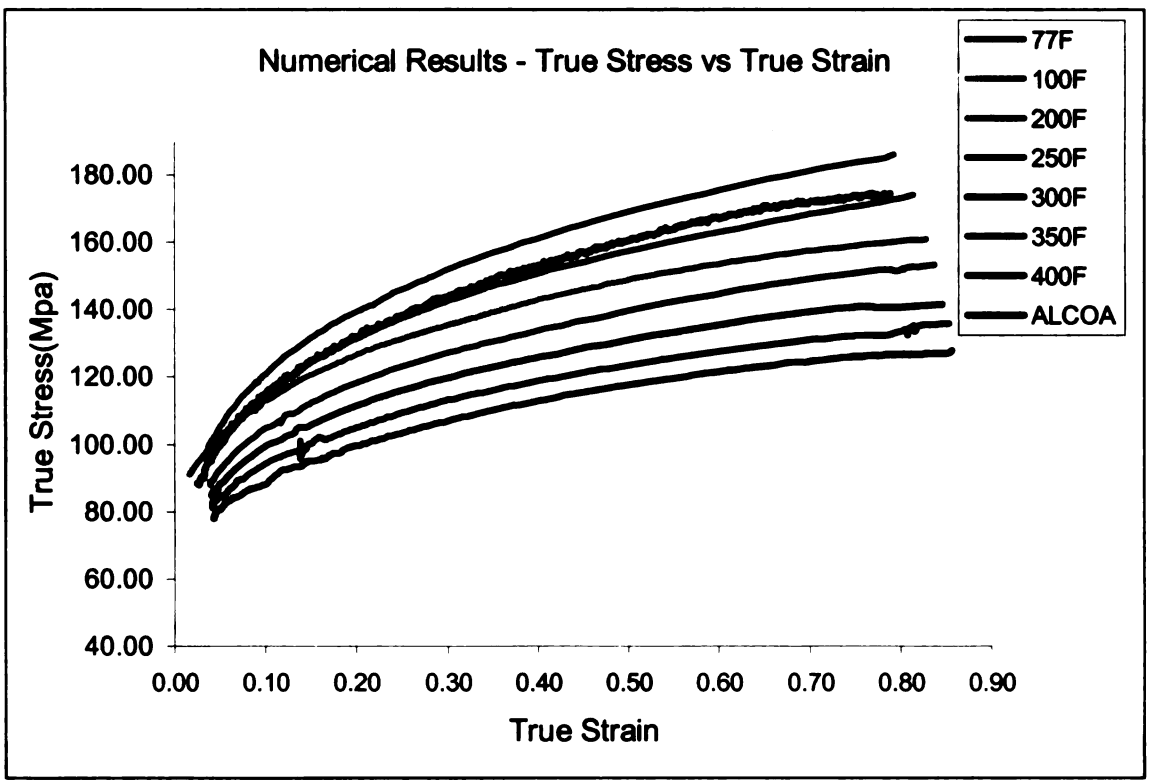

Fig 5.10 shows the Numerical results obtained at room temperature and elevated temperatures.

As seen from Fig. 5.11 ALCOA's experimental stress-strain curve matches the numerical result for 100F better than for 77F (room temperature). This could be due to the excessive heating of the aluminum sheet during the experimental process. Although in each experiment care is taken to make sure the temperature of the specimen stays constant during the experiment, it is very difficult to maintain an isothermal condition. It is also not known what the temperature of the lab was at the time the experiment was performed at Alcoa.

In all the above experimental results the strain rate was assumed to be constant at room temperature even though strain rate control was not applied. This is because aluminum is known to be strain rate insensitive at room temperature.

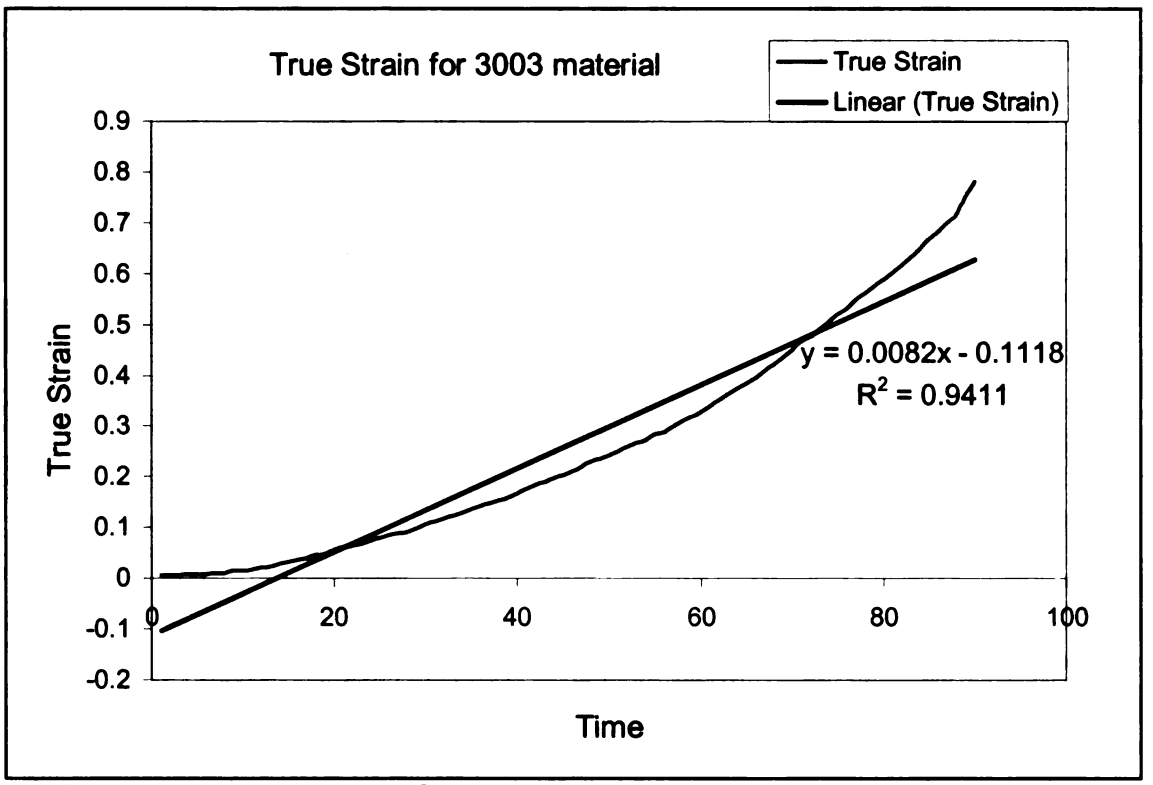

Fig 5.11 shows the plot of experimentally obtained true strain without the application of strain rate control algorithm

Fig. 5.12 shows the plot of experimentally obtained true strain without the application of strain rate control algorithm. It can be seen that at room temperature the differences are small. For tests which will be conducted at higher temperature, the strain rate parameter becomes important and hence the strain rate control algorithm must be applied.

An attempt was made to control the strain rate at room temperature using the strain rate control algorithm mentioned before, but due to some limitations of the equipment used for this test, accurate control of the strain rate near the pole of the hemisphere was not possible. Fig 5.13 below shows the strain plot with the strain rate control algorithm incorporated.

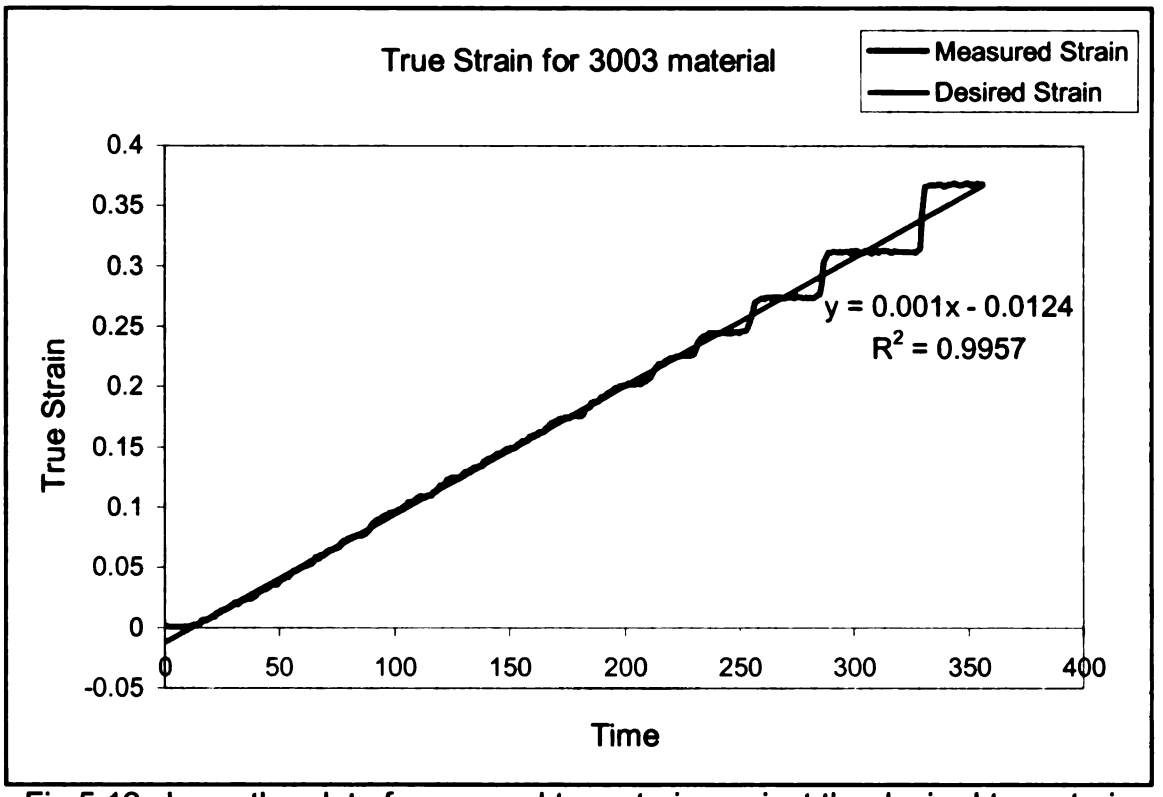

Fig 5.12 shows the plot of measured true strain against the desired true strain with the strain rate control algorithm incorporated.

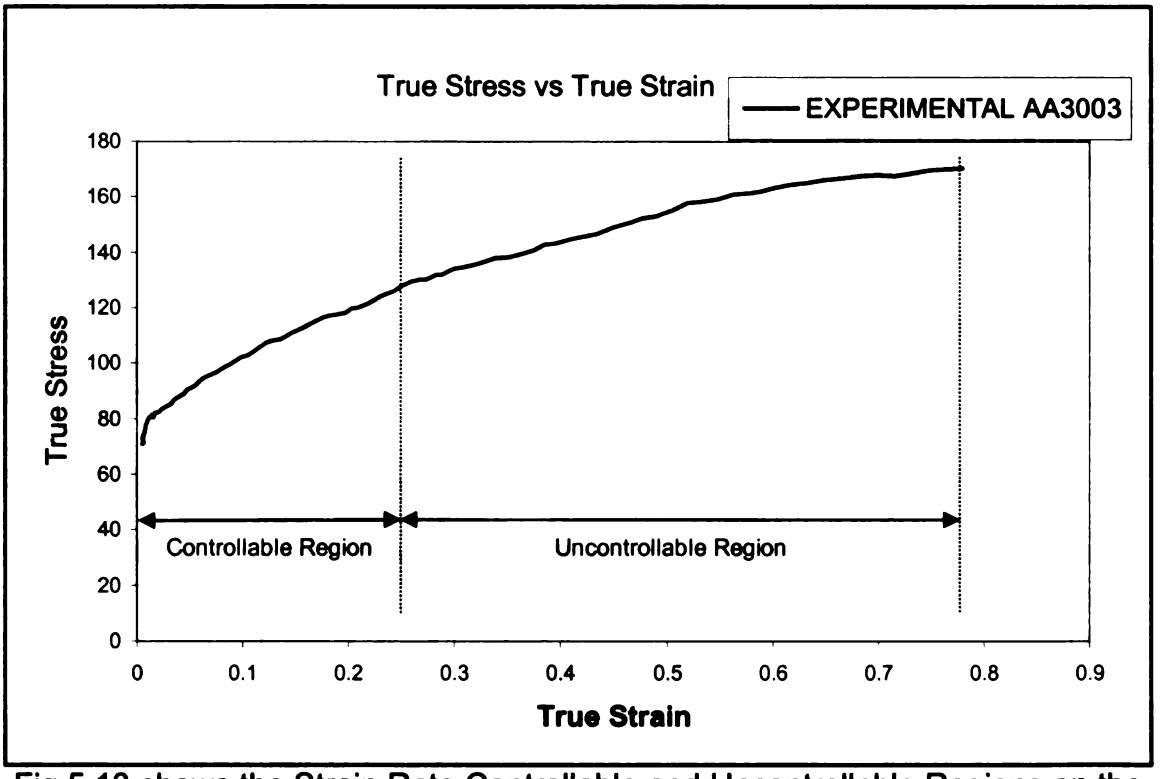

Fig 5.13 shows the Strain Rate Controllable and Uncontrollable Regions on the Strain Curve with the Present System

As seen from fig 5.13 above, the measured strain follows the desired strain accurately for the initial part of the experiment when the rate of of plastic deformation near the pole of the hemisphere is high However, as the rate of plastic deformation decreases, the low resolution of the ER3000 pressure controller and also that of the vertical LVDT (spherometer) make it impossible to accurately control strain rate. Low plastic deformation requires providing pressure in very small increments, and diaphragm based ER3000 pressure controller is not capable of providing small pressure increments. In the future, for accurate control of strain rate, the present ER3000 pressure controller must be replaced by a servo valve and the present LVDT used for the spherometer must be replaced with a higher resolution model.

However the ER3000 model does have the capability to control the pressure accurately when a predetermined pressure profile is input to the controller. This technique was tried and a theoretically determined pressure profile based on regression analysis was input to the controller. The result from this was identical to that in figure 5.13, and so to obtain a fully controllable strain profile a series of theoretically determined pressure profiles have to be input which will represent the desired strain curve. This technique however requires determining the theoretically calculated pressure profiles and is specific to a particular material, strain rate and temperature. So this technique is good for the present system but it fails to work when a material with an unknown theoretical pressure profile has to be tested.

The servo valve technology has the advantage of easy communication with the computer and also has the capability of controlling pressure with high accuracy and resolution. A Servo-Proportional Valve manufactured by MOOG, Inc which has a flow rate of about 1GPM and has electrical feedback capability is a good choice for this application.

As mentioned before, the failure in the numerical model was predicted using the forming limit diagram (FLD). The FLD was plotted using the LS-Dyna's post processor, LS-Post, which has the built-in capability of plotting minor and major strains in the forming limit diagram. The forming limit diagram was plotted for the 3003 material at room temperature and elevated temperature to obtain the failure point in the analysis. For higher temperatures the forming limit curve increases, suggesting that the AA3003 material can be deformed to higher strains before failure occurs. Figure 5.14 shows the FLD and associated strains developing in the bulged sheet. Figure 5.15 shows the predicted shape while Fig. 5.16 shows the actual deformed shape of the bulged aluminum sheet. According to Fig. 5.14, the bulged sheet fails in two locations; near the pole of the hemisphere where deformation is balanced biaxial, and near the clamped edge where deformation is uniaxial. The actual part shown in Fig. 5.16, fails near the pole.

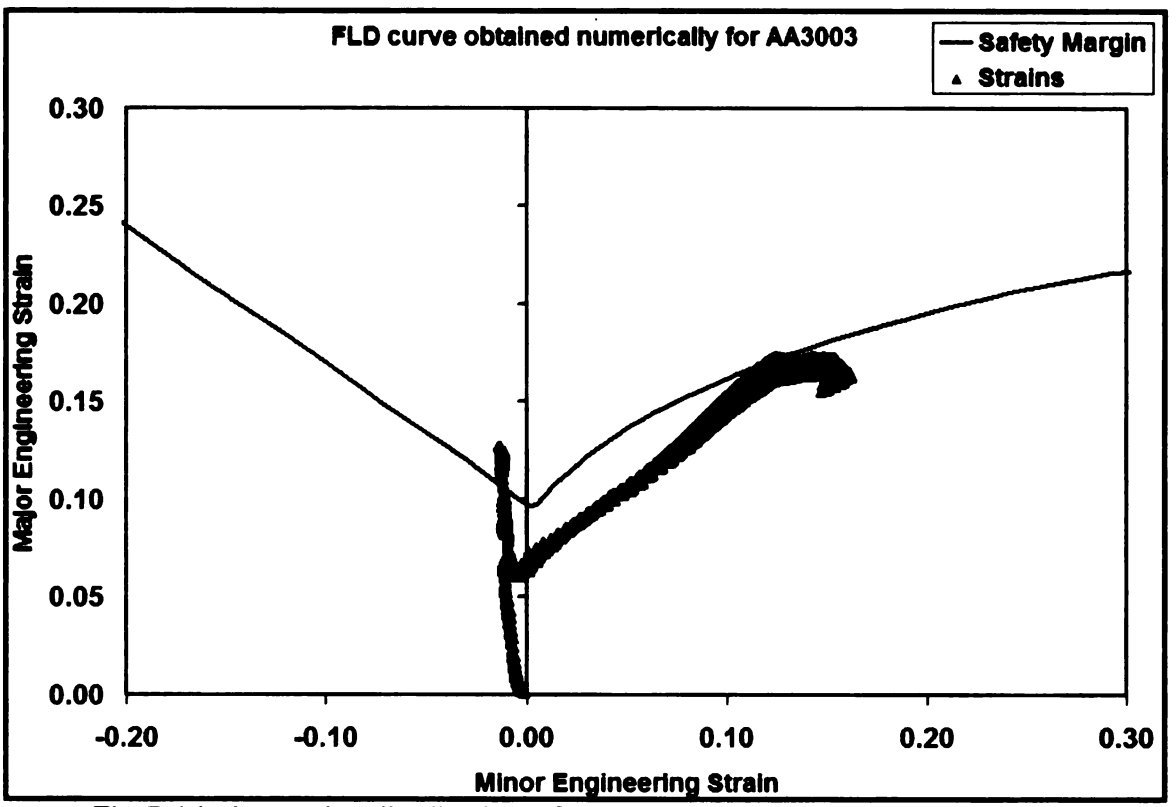

Fig 5.14 shows the distribution of major and minor strains on the FLD the sheet failed where the strains crossed the FLD curve

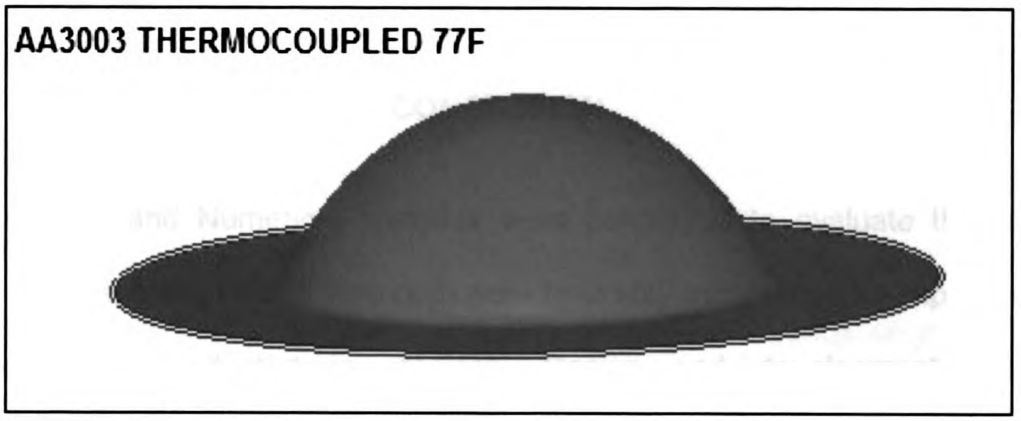

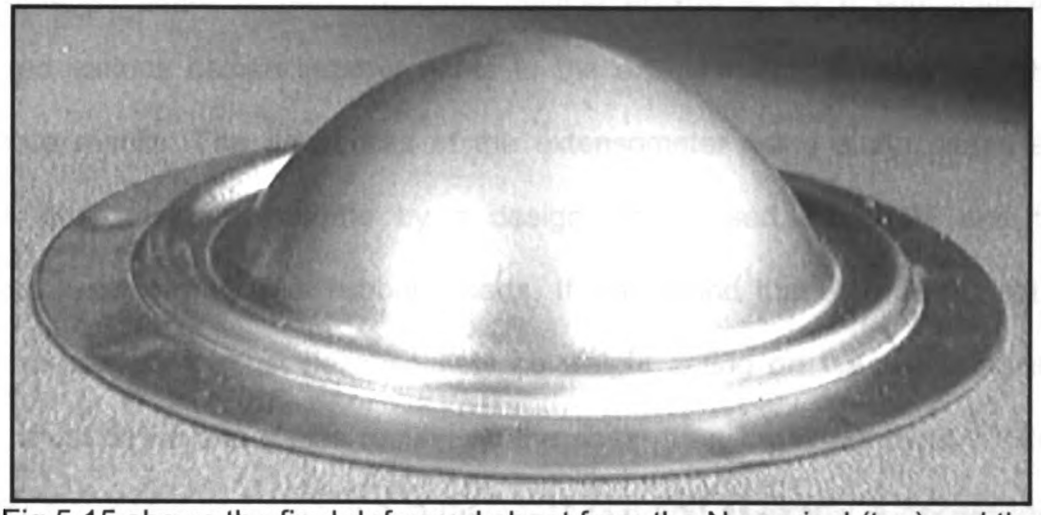

Fig 5.15 shows the final deformed sheet from the Numerical (top) and the Experimental (bottom) tests

CHAPTER 6

CONCLUSION

Experimental and Numerical analyses were conducted to evaluate the sheet bulging process and results from both were favorably compared with experiments independently conducted by ALCOA. Design and development of the experimental setup to perform sheet bulging proved to be a challenge and required various design improvements to the extensometer in order to obtain accurate results. The drawbacks of the extensometer using strain gages and single probe were overcome by a design which used an LVDT and two extensometer probes with rubber inserts. It was found that in order to obtain good results there must be absolutely no weight acting on the specimen and there must be no sharp pins resting on the sheet as it would puncture it. Great attention to detail and precision in manufacturing and assembly is necessary in order to obtain the desired result.

The numerical analysis was conducted with Ls-Dyna 3D using the material model proposed by Barlat et al. (1997, YLD96). The UMAT written for this material model was modified by Aberdrabbo [9] in order to account for sheet forming at elevated temperature. This model will be used in the future to compare numerically predicted sheet bulging results with those obtained experimentally at elevated temperature. It was found that numerical results are in good agreement with the experimental results and can be used in confidence as a robust finite

element code to predict various deformation parameters of the sheet bulging process.

The slight discrepancy between the experimental results obtained at MSU and ALCOA were attributed to material hardening/aging, absence of strain rate control at room temperature, and possible difference in ambient temperature at which the tests were conducted at MSU and ALCOA (i.e., 77 F vs. 100 F) .

CHAPTER 7

SCOPE OF FUTURE WORK

As seen from the numerical results, the formability of aluminum increases as the temperature is increased. Therefore, the next step in the sheet bulging study would be to design the system to conducts tests at elevated temperatures. Since aluminum is strain rate sensitive at elevated temperatures, the presently used ER3000 pressure controller must be replaced by a servo valve which has a higher resolution and is able to control the pressure more precisely.

The present system has the capability to withstand temperatures of up to 220 C (428F) for 10 minutes. This shortcoming has to be improved by using materials which have better temperature resistance for the LVDT body, cable, etc., if conducting bulging test at temperatures higher than 500 F is required. To improve the sensitivity of the system, two LVDT's can be used individually to detect displacement of each extensometer probe.

The present system can be modified slightly by using another extensometer to measure the strain along two orthogonal directions; this is particularly useful for conducting tests on anisotropic materials. Once a successful strain rate control has been designed different strain profiles can be applied and observed to see how this affects the final deformation of the sheet. This capability combined with the high temperature capability will be an excellent test machine for studying the biaxial behavior of various materials.

REFERENCES

[1] J L Duncan, J Kolodziejski, G Glover, "Bulge testing as an aid to formability assessment". Proc. I.D.D.R.G 10th congress, Warwick, 1978, P317.

[2] K Siegert and S Wagner, "Formability characteristics of Aluminum sheet", TALAT – Training of Aluminum application technologies Lecture 3701.

[3] M Atkinson, "An investigation of hydraulic Bulging as a Biaxial Straining test for sheet metal"

[4] Robert H. Wagner and Jean-Loup Chenot, "Fundamentals of metal Forming" , John Wiley ans sons, Inc.

[5] ALCOA technical center report on Sheet Bulge testing.

[6] Nader E Abedrabbo, "Experimental and Numerical Investigation of stamp hydroforming and ironing of wrinkling in sheet metal forming" – A master's thesis submitted to Michigan State University 2002.

[7] Nader E. Abedrabbo, "Forming of aluminum alloys at elevated temperatures" – A Phd thesis submitted to Michigan State university 2005.

[8] Nader E Abedrabbo, Farhang Pourboghrat, John Carsley, "Forming of aluminum alloys at elevated temperature – Part 1: Material Characterization" International Journal of Plasticity, 22 (2006) 314-341.

[9] Nader E Abedrabbo, Farhang Pourboghrat, John Carsley, "Forming of aluminum alloys at elevated temperature – Part 2: Numerical Modelling and Experimental verification" International Journal of plasticity, 22 (2006) 342-373.

[10] D E Green, K W Neale, S R MacEwen, A Makinde, R Perrin, "Experimental investigation of the biaxial behavior of an aluminum sheet" International Journal of Plasticity - 20 (2004) 1677–1706

[11] Daoming Li, Amit K Ghosh, "Biaxial warm forming behavior of aluminum sheet alloys". Journal of materials processing Technology – 145(2004) 281 292

[12] F Bron, J Besson, "A yield function for anisotropic materials application to aluminum alloys" International Journal of Plasticity - 20 (2004) 937–963

[13] LSTC website – www.lstc.com

[14] Zampaloni M., Abedrabbo N. and Pourboghrat F. "Experimental and Numerical Study Of Stamp Hydroforming Of Sheet Metals" International Journal of Mechanical Sciences, 45 (2003) 1815-1848.

[15] Zampaloni M. "Experimental and Numerical Study of Stamp Hydroforming for Processing Glass Mat Fiber Reinforced Thermoplastic Sheets", Master of Science Thesis, Michigan State University, 2000.

[16] R Hill, "A theory of the Plastic Bulging of a Metal Diaphragm by Lateral Pressure", Phil. Mag Ser 7, Vol. 41, No 322, 1950, P1133

[17] Amit Mukund Joshi, "Strain studies in sheet metal forming" – A study on sheet metal forming.

[18] Lars Pilgaard Mikkelson, "Thickness effects in membrane solutions in sheet metal forming"

[19] G Thomas Mase, George E Mase. "Continumm mechanics for Engineers" second edition, CRC Press LLC.

[20] JC Simo, TJR Hughes, "Computational Inelasticity (Intermediary applied mathematics" Springer Publications.

[21] Barlat, F., Maeda, Y., Chung, K., Yanagawa, M., Brem, J. C., Hayashida, Y., Lege, D. J., Matsui, K., Murtha, S. J., Hattori, S., Becker, R. C., Makosey, S., 1997. Yield function development for aluminum alloy sheets. J. Mech. Phys. Solids 45 (11/12), 1727–1763.